MdfA – A model multidrug efflux pump for single-molecule investigations of transport.

By Stephanie Sabina Nagy

A thesis submitted in partial fulfilment of the requirements for the degree of

Master of Research

Department of Chemistry and Biomolecular Sciences

Macquarie University

9th of October 2017

Table of Contents

Disclaimer

I certify that the research presented in this thesis is my own original work. All other work is clearly stated and referenced throughout this thesis.

I certify that this thesis has not been submitted for a higher degree to any other university or institution other than Macquarie University, Sydney, Australia.

Research was undertaken with approval as a Notifiable Low Risk Dealing by the Institutional Biosafety Committee (IBC) effective 6th of February 2015. IBC reference number: 5201401141.

Stephanie S. Nagy
9th of October 2017

Acknowledgements

First, I would like to thank to my supervisors Professor Ian Paulsen and Dr. Karl Hassan for the exciting opportunity to conduct this research in the Paulsen laboratory. I would like to especially thank them for the support, advice and positivity provided that has made this research a pleasant experience. I would also like to sincerely thank Professor Antoine van Oijen, Dr. Andrew Robinson and the van Oijen laboratory group from the University of Wollongong for their warm welcome and provision of time, expertise and equipment to assist in the development of a single-cell transport assay. I would also to thank Professor Eitan Bibi, from the Weizmann Institute of Science, for the kind donation of *E. coli* UTL2*mdfA::kan* strain and MdfA and MdfA_CL_V44C/V307C plasmids. Special thanks to Sue Lindsay from the Microscopy Unit, Macquarie University for the advice and training regarding scanning electron microscopy and Dr. Bhumika Shah for her mentorship and advice regarding protein purification. I would also like to especially thank the students and post-docs of the Paulsen lab for their collegiality and support. Finally, I would like to thank my family and friends, for the support and understanding they have provided me throughout this project.

Abstract

MdfA is an *Escherichia coli* multidrug efflux pump that has a broad-substrate profile that encompasses cationic, neutral and zwitterionic antimicrobials. MdfA is proposed to operate by an alternating access mechanism, a major substrate translocation mechanism thought to occur throughout a diverse range of transport proteins. However, direct visual evidence for this transport mechanism has not been obtained for any protein. The aim of this research is to explore MdfA as a model for conducting single-molecule Förster resonance energy transfer (sm-FRET) experiments to allow for direct visualisation of the alternating access mechanism, by direct observation of fluorescent substrate transport in parallel with protein domain movement. A prerequisite for this work is to identify a highly fluorescent substrate. This thesis aimed to determine whether MdfA and a Cys-variant of MdfA designed for FRET studies can recognise and transport the highly fluorescent monovalent cation rhodamine 6G (R6G) using fluorescence binding and transport assays. The results demonstrate that R6G is a substrate of MdfA, and that the Cys-variant of MdfA retains sufficient activity as a model for future sm-FRET studies. Moreover, this thesis reports on the first direct visualisation of fluorescence transport mediated by a multidrug efflux pump at the single-cell level in real-time.

.

Chapter 1. Introduction

1.1. Transporters

Transporters are essential to all domains of life and play a fundamental role as the essential gatekeepers of the cell. Integral membrane transporters provide a direct pathway across the membrane to mediate the exchange of a diverse range of biologically active ions, molecules and macromolecules, across a largely impermeable lipid bilayer for cell survival (1). Hence, transport proteins are fundamental to a range of essential cellular processes including nutrient import, toxin export, energy-conservation, cellular homeostasis and chemical defence mechanisms (2). Transporters represent one of the largest and most diverse classes of proteins and are currently classified into four major transporter classes based on their mode of transport, energy-coupling mechanism, substrate specificity and molecular phylogeny, including channels, group translocators, primary active transporters and secondary active transporters (3).

Membrane channels function to facilitate the passage of a restricted number of ions (ion channels), water molecules (aquaporins) and small solutes down a concentration or electrochemical gradient, and represent the only membrane transporters that are energy-independent (1). These transporters function to translocate substances close to the diffusion limit, requiring minimal conformational changes to facilitate rapid substrate turnover within the cell (2). Channels represent 2-8% of total transporters in prokaryotes and up to ~43% in eukaryotes (3).

Group translocators are the only transporter class to modify substrate during import and couple phosphoenolpyruvate (PEP) as a source of energy and phosphate to selectively phosphorylate sugars during import (4). These proteins only represent a small percentage ~1-11% of transporters in bacteria (3).

Primary active transporters drive the transport of a diverse range of substrates against a thermodynamically unfavourable electrochemical gradient by coupling substrate translocation with a primary energy source, commonly ATP-hydrolysis (4,5). Primary transporters are most prevalent in prokaryotes, representing 30-52% of transporters (3).

Secondary active transporters harness free energy stored in electrochemical gradients, most commonly coupling the proton-motive force or sodium-motive force to translocate an extensive range of molecular species against a concentration or electrochemical gradient (2). This class forms the one of the most abundant classes of transporter, constituting 50% of all membrane transport systems in

eukarya and archaea and up to 58% in bacteria (3). Together, with primary transporters, they typically represent up to 90% of transporters encoded within prokaryotic or eukaryotic genomes (3).

1.2. The alternating access mechanism of active transport

The alternating access mechanism is proposed to be the mechanism of action of most primary ABC transporters and secondary active transporters (2,5). In this mechanism of transport, the accessibility of the substrate-binding site is asynchronous (6). Substrate transport described under the alternating access mechanism must undergo two distinct conformational changes – inward-facing and outward-facing, whereby the transition from one state to the other occurs via an occluded state (Figure 1) (6).

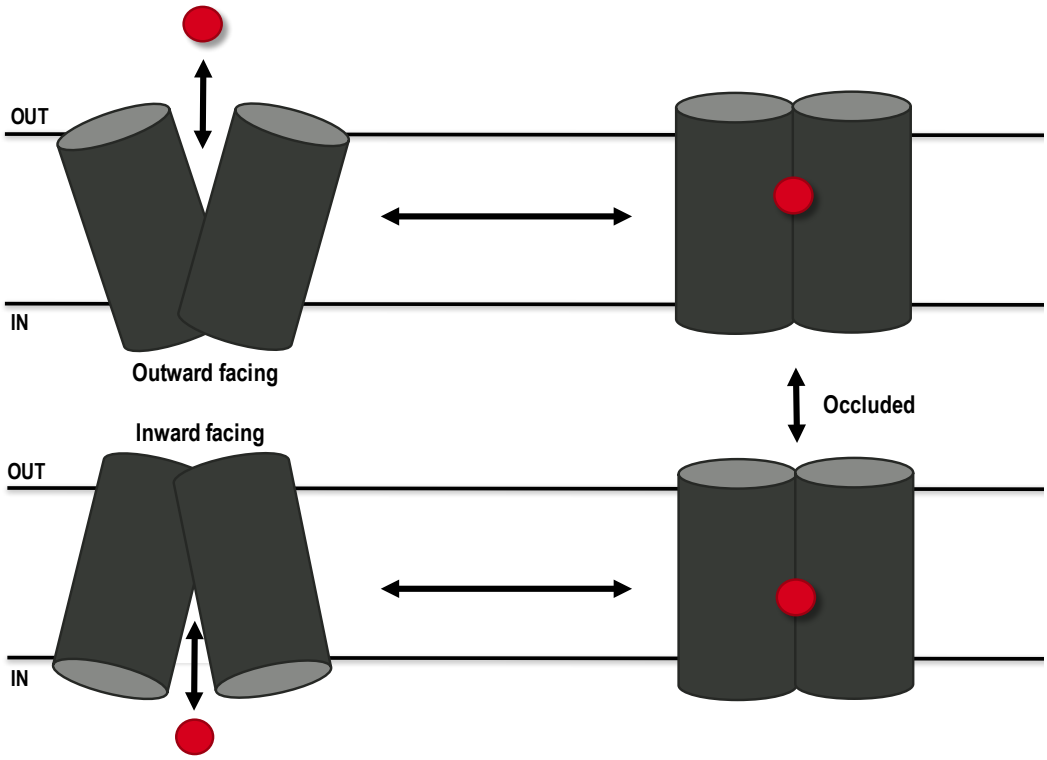

Figure 1. Schematic illustration of the alternating access model of transport. In the alternating access mechanism of transport, a transporter will translocate substrate in two major states – an outward-facing and inward-facing state. The transition between inward-facing and outward-facing states must occur through an intermediate occluded state.

To assign the alternating access model, a transporter must fit three distinct criteria – 1) a transporter must contain a cavity in the interior of the transporter to fit a small molecule; 2) a transporter must assume two distinct configurations so that the binding site is not exposed at either end of the membrane at the same time; 3) the affinity of the substrate to the binding site must change between the two configurations of the transporter to facilitate substrate uptake and release (6). The alternating access mechanism only represents a generalised model of active transport of which a myriad of distinct active transport processes can be described under (2,7). Hence, a precise understanding of

how transporters may perform the alternating access mechanism is essential to understanding the role of an active transport protein in fundamental cellular biology and in disease.

1.3. Molecular mechanisms of antibiotic resistance

Antimicrobial resistance (AMR) represents one of the greatest threats to global health (8). The rise and spread of bacterial AMR and multidrug resistance can be largely attributed to four independent molecular mechanisms that are selected for under antibiotic challenge (9,10).

1.3.1. Inactivation of antibiotics

The first method is direct inactivation of an antibiotic by degradation or modification of the functional group of the antibiotic. The expression of hydrolytic enzymes in the periplasmic space of Gram-negative bacteria (β-lactamases, extended-spectrum β-lactamases or carbapenemases) mediates direct breakdown of the β-lactam class of antibiotics before they can reach their target (9,11–13). Bacteria may also inactivate an antibiotic by direct modification of the antibiotic to prevent binding of an antibiotic to a bacterial target by steric hindrance (9). This mechanism is a primary mechanism in aminoglycoside resistance, as these antibiotics are readily inactivated by enzymatic phosphorylation, acetylation or adenylation that render them inactive against their target by the reduction of net charge (10,15).

1.3.2. Target modification or bypass

Bacteria also promote cell survival under antibiotic challenge by mutational resistance or alteration of the antibiotic target to circumvent antibiotic binding. This mechanism is well represented by methicillin-resistant *Staphylococcus aureus* (MRSA), which produces a modified form of the periplasmic binding protein (PBP) known as PBP-2A in the presence of methicillin and β-lactams (9,16). Alternatively, modification of the rRNA subunit in bacteria is a common target for modification. Methylation of the 23S rRNA in *Staphylococcus aureus* confers resistance by inducing a conformational change to the binding site of a broad range of ribosome-binding antibiotics (9,17). Bacteria may also develop resistance by target bypass. This mechanism of resistance is well-represented in trimethoprim (TMP) resistance. TMP directly inhibits the enzyme dihydrofolate reductase (DHFR) that converts dihydrofolate to tetrahydrofolate for the synthesis of amino acids and purines essential for cell survival (18). In TMP-resistant *S. aureus* and *Streptococcus pneumoniae*, a single amino acid modification in the promotor region of the *dhfr* gene leads to the overproduction of DHFR (18). The overproduction of the DHFR enzyme allows for the target to outcompete the antibiotic, allowing for the resistant organism to directly bypass the effect of the antibiotic to continue the folate biosynthesis pathway and promote survival under antibiotic challenge (18).

1.3.3. Decreased permeability

The first line of physical defence against antibiotics lies in the permeability of the bacterial cell surface. Gram-negative bacteria are intrinsically less susceptible to antibiotic challenge due to the presence of a rigid outer-membrane, composed of lipopolysaccharide (LPS) that demonstrates significantly less fluidity than traditional glycerophospholipid found in the most plasma membranes (19). Thus, these features of LPS successfully limits the rapid penetration of the outer-membrane by lipophilic antibiotics (19). In contrast, the mesh work of the thick peptidoglycan layer of Gram-positive bacteria is fluid and coarse and therefore it offers minimal protection against free diffusion of antibiotic substances (19). However, hydrophilic antibiotics may still enter Gram-negative bacteria by non-specific outer-membrane porins that target small molecules (20). Hence, a common mechanism to confer resistance to hydrophilic antibiotics in Gram-negative bacteria is to down-regulate porin expression and/or exchange outer-membrane porins for smaller, more specific porins to reduce permeability of antibiotics into the cell (9). This mechanism has been well-documented for nosocomial, opportunistic pathogens such as *Pseudomonas aeruginosa* and *Acinetobacter baumannii* (9,21,22).

1.3.4. Active extrusion of antibiotics

Bacteria may also reduce the accumulation of antibiotics by overexpressing active transporters to directly efflux noxious compounds out of the cell (9). Active extrusion of antibiotics by efflux pumps represents the most ubiquitous form of antibiotic resistance across Gram-positive and Gram-negative bacteria (23). The rapid extrusion of antibiotics and other noxious compounds allows for bacteria to reduce the intracellular concentration of an antibiotic to sub-therapeutic concentrations, thereby promoting the survival of bacterial populations under antibiotic challenge.

1.4. Multidrug efflux pumps

Bacterial multidrug resistance can arise from the acquisition of multiple independent mechanisms of antibiotic resistance on mobilised genetic elements such as resistance plasmids or by the overexpression of multidrug efflux pumps (10). Transport proteins are often defined by their selectivity for a singular substrate or substrate class (24). However multidrug efflux pumps are unusual in that they demonstrate multi-specificity to transport a diverse range of chemically unrelated therapeutics (24). Hence, the over-expression of these intrinsic efflux pumps and mobilisation of these transporters on resistance plasmids have been implicated as one of the primary mechanisms of bacterial multidrug resistance (10,25). Currently, there are six phylogenetically and mechanistically distinct bacterial multidrug efflux classes that have been defined- the resistance-nodulation-division (RND) family, the ATP-binding cassette (ABC) superfamily, the multidrug and toxic compound

extrusion family (MATE), small multidrug resistance (SMR) family, the major facilitator superfamily (MFS) and proteobacterial antimicrobial compound extrusion (PACE) family (26,27). A schematic illustration of each class is represented in Figure 2.

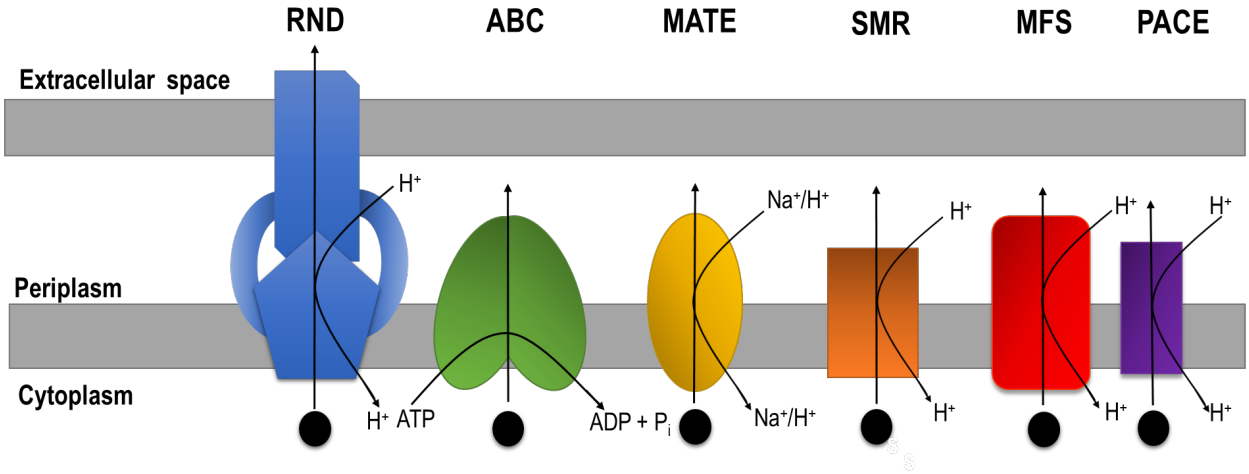

Figure 2. Schematic illustration of the six multidrug efflux pump classes. The RND family, ABC family, MATE family, SMR family, MFS family and PACE family and their principal energy-coupling mechanism of active transport. Figure adapted from Blanco *et al*., 2015 (23).

1.4.1. Resistance-Nodulation-Division (RND) Family

The RND family of multidrug efflux pumps represent one of the most important multidrug resistance determinants in Gram-negative pathogens due to the capacity to export noxious compounds directly across the double-membrane of the cell (28). Some members of this family of transporters are constitutively expressed and thus contribute to intrinsic multidrug resistance of Gram-negative pathogens. These efflux systems function as tripartite transporters, typically being composed of an inner membrane RND protein, a membrane fusion protein (MFP), and an outer-membrane factor (OMF) to provide a direct pathway for substrate translocation across the double-membrane of the cell. These complexes are proposed to associate in a 3:6:3 stoichiometry (29) (Figure 3). RND-efflux pumps are predicted to operate via a peristaltic pump mechanism (30). In this mechanism, the protomers within the inner-membrane protein rotate via three defined conformational states from access, binding and extrusion that has been seen in crystal structures of the *Escherichia coli* RND protein AcrB in three distinct conformational positions (31). In a single cycle of substrate transport, the deep binding pocket of the porter domain of AcrB is exposed to the periplasmic face for substrate binding. Substrate binding in the transmembrane domain triggers an outward-open conformation to allow water molecules to come close to the protonatable residues (32). This structural arrangement triggers an inward facing conformation of the transmembrane domain to release protons to the cytoplasm face whilst simultaneously triggering the outward-open conformation of the porter domain for substrate release into the TolC channel for substrate extrusion (32).

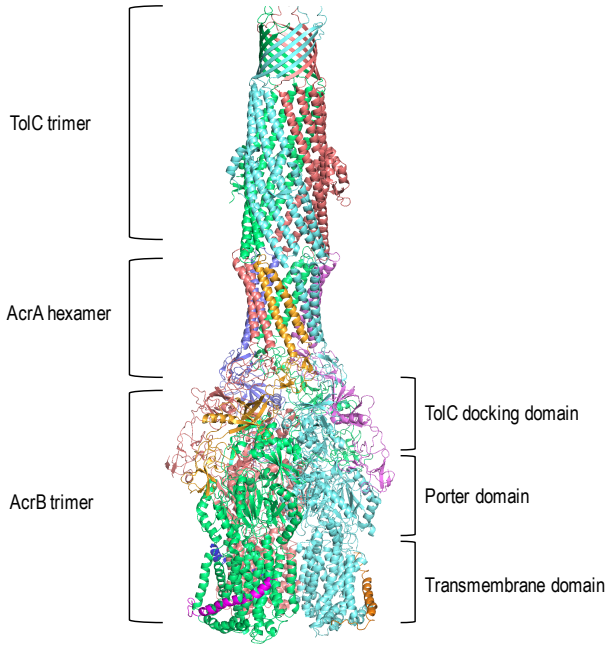

Figure 3. Cryo-electron microscopy structure of AcrAB-TolC RND complex of *E. coli* [PDB: 5NG5](33). Structure of an RND efflux complex comprised of a tripartite RND efflux pump (AcrB), hexameric membrane fusion protein (AcrA) and trimeric outer-membrane fusion protein (TolC). Figure made in PyMOL.

1.4.2. ATP-binding cassette (ABC) superfamily

The members of the ATP-binding cassette (ABC) superfamily represent one of the largest classes of transporters across all domains of life (5). Members of the ABC superfamily were shown to be composed of two highly-conserved nucleotide binding domains (NBD) and two variable transmembrane domains (TMD)(5). The X-ray crystal structure of SAV1866, the first structure of bacterial ABC multidrug efflux pump from *S. aureus* defined critical structural features of bacterial ABC efflux pumps (34), whereby ATP-binding was localised at the interface of the two NBD domains, whilst the two TMD domains provided a deep substrate-binding cavity to facilitate drug transport across the membrane (Figure 4) (34). Structures of ABC exporters in the inward-facing, outward-facing and occluded states provide significant structural evidence for a proposed alternating access mechanism of transport (34–36). In this mechanism, an ABC exporter is proposed to rest in the inward-facing state, whereby the substrate binding cavity is accessible in the cytoplasmic space for substrate loading in the absence of nucleotide or with ADP bound (37). ATP binding at the interface of the two NBD domains triggers NBD dimerization, followed by a conformational change from inward-facing to outward-facing state, via an intermediate occluded state (37). Substrate is released upon loss of binding affinity to the substrate binding site. ATP-hydrolysis triggers the reversion of the ABC transporter from outward-facing to inward-facing to prepare for another cycle of transport (37).

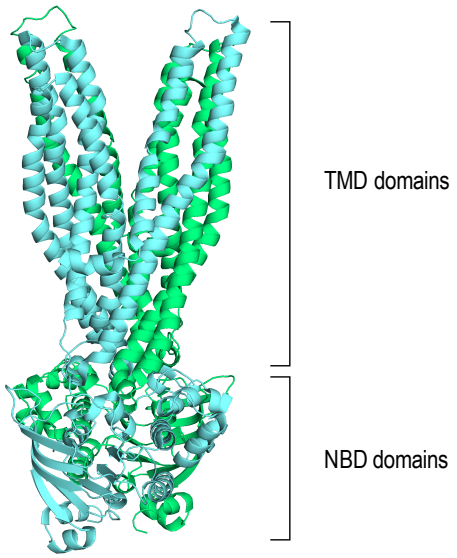

Figure 4. X-ray structure of the SAV1866 of *S. aureus* [PDB: 2ONJ](38). Structure demonstrates canonical organisation of a ABC transport homodimer composed of two TMD domains, a central cavity for substrate translocation, and two NBD domains for ATP-hydrolysis. Figure made in PyMOL.

1.4.3. Multidrug and Toxic Extrusion (MATE) Family

The MATE family of multidrug efflux pumps are primarily cationic and lipophilic compound exporters (39). MATE family members can either be proton or sodium gradient energy-dependent (40–42). Structurally, the MATE family members are single-component efflux pumps composed of a twelve transmembrane α-helical core that consist of two domains (N-terminal and C-terminal) to yield a central hydrophobic cavity for substrate transport (43) (Figure 5). Transport is predicted to be triggered upon the binding of a cation (H^+ or Na^+) to a conserved cation-binding domain in the resting outward-facing conformation of the transporter (40,43). Binding triggers a conformational switch from outward-facing to inward-facing for cation-exchange with substrate and release of ion into cytoplasm to drive inward-facing to outward-facing conformational change for substrate release into the periplasm/extracellular space upon loss of binding affinity to the binding cavity (40,43). However, the MATE family efflux proteins have only been captured in outward-facing conformation (41,43,44). Thus, an inward-facing crystal structure of a MATE transporter is required to provide further structural evidence for this putative alternating access mechanism of substrate transport facilitated by the MATE family of efflux pumps.

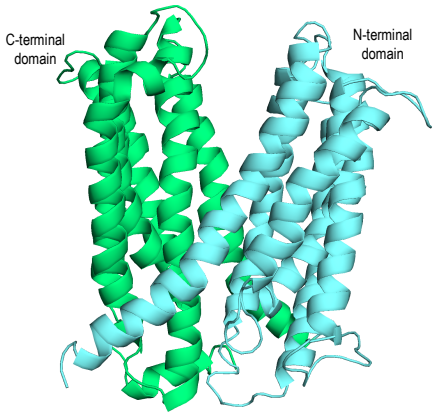

Figure 5. X-ray structure of NorM of *Vibrio cholera* [PDB: 3MKU](43). Structure reveals outward-facing conformation of a single-component MATE pump. NorM is organised in archetypal twelve-transmembrane helices, revealing a large central cavity divided by the N-terminal domain and C-terminal domain for substrate translocation. Figure made in PyMOL.

1.4.4. Small Multidrug Resistance (SMR) Family

Proteins in the SMR family are proton-motive force driven multidrug efflux pumps and have defined substrate profiles for quaternary cationic compounds (QCCs) (45,46). SMR efflux pumps are restricted to the prokaryotic phyla and are often localised encoded on mobile genetic elements such as plasmids or integrons (46). The SMR family encode for the smallest multidrug family members, at ~110 amino acid residues in length (46). The SMR efflux pump is comprised of two protomer units composed of four transmembrane α-helices that dimerise in an antiparallel fashion to yield an eight transmembrane α-helix core homodimer for $2H^+$/drug antiport across the lipid bilayer (47–50) (Figure 6). Transport is proposed to occur via a single-site alternating access model (49). In a single cycle of transport, the binding of two protons is predicted to trigger a conformational switch from outward-facing to inward-facing to exchange with cationic substrate via direct competition (49). The binding of substrate to the single binding site is predicted to induce conformational change to the outward-facing state for substrate release (49)

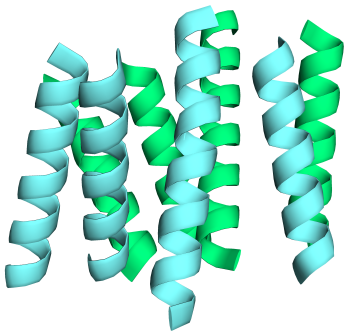

Figure 6. Cryo-electron microscopy structure of EmrE of *E. coli* [PDB:2I68](51). Cryo-EM structure reveals archetypal antiparallel arrangement of the SMR homodimer composed of eight transmembrane α-helices. Figure made in PyMOL.

1.4.5. The Major Facilitator Superfamily (MFS)

The MFS represent the largest family of secondary active transporters and are essentially ubiquitous to all domains of life (52). MFS members for which structural information is available each have a homologous structure. Members of the MFS efflux pumps function as single-component twelve (or fourteen) transmembrane α-helices connected by hydrophilic loops (46,53,54). In MDR MFS members, the division between the N-terminal and C-terminal domain of multidrug efflux pumps reveals a centralised, hydrophobic core that contains a substrate binding site at the apex of the deepest end of the central cavity (55,56) (Figure 7). This cavity has been shown to harbour the critical acidic residues required for cationic substrate binding and transport catalysis across the lipid bilayer. The MFS fold consists of two pseudo-symmetrical six-helical bundle domains, composed of a two-fold inverted repeat of three helices each (54). This arrangement yields two rigid bodies to undergo the rocker-switch alternating access mechanism (7). Crystal structures of MFS members captured in outward-facing, occluded and inward-facing conformations is suggestive of a common alternating access mechanism of substrate transport (55–57).

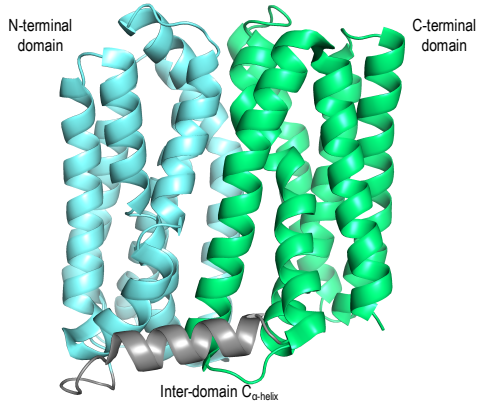

Figure 7. X-ray structure of MdfA of *E. coli* [PDB:4ZOW](56). Structure of single-component efflux pump MdfA. Structure reveals representative twelve transmembrane α-helices divided into a N-terminal and C-terminal domain to produce a centralised hydrophobic binding cavity for transport. Figure made in PyMOL

1.4.6. Proteobacterial Antimicrobial Compound Efflux (PACE) Family

PACE family members represent the most recent multidrug efflux family to be identified. A recent study led by Hassan *et al*., revealed the novel multidrug efflux pump AceI, to confer resistance to bisbiguanide antiseptic chlorhexidine (58). Further studies led to the identification of AceI orthologues across γ- and β-proteobacterial species confer elevated resistance to chlorhexidine when overexpressed in *E. coli* (27). Members of the PACE family are conserved amongst proteobacterial genera and demonstrate a conserved sequence to encode for two tandem bacterial transmembrane pair (BTP) domains. Characterisation of AceI homologues heterologously expressed in *E. coli* has shown them to confer resistance to an array of biocides, validating the newly discovered PACE family

members as multidrug efflux pumps (27). However, the structural characterisation of the PACE family members is yet to be determined.

1.4.7. Limitations to the study of multidrug efflux pumps

At the heart of the transport mechanism of multidrug efflux pumps, lies the common mode of the alternating access mechanism. Despite the rapid expansion of newly discovered multidrug efflux pumps and following extensive structural and biochemical characterisation of these efflux pumps, the direct observation of the conformational events that drive transport has not been directly observed. Traditional structural techniques such as X-ray diffraction crystallography, nuclear magnetic resonance spectroscopy and cryo-electron microscopy have been utilised to characterise the alternating access mechanism of these transporters (59–62). However, these techniques can only provide a static representation of a structure of an inherently dynamic transport process. Molecular dynamics has proved to be a powerful approach to predicting conformational dynamics based on high-resolution crystal structures of a protein (63,64). While an *in silico* approach can provide support for the conformational dynamics of a protein, it does not provide direct experimental verification of the mechanism. Ensemble biochemical and biophysical techniques have shed insight onto dynamic nature of the conformational dynamics in these proteins (59–62). However, the ensemble averaging means that the transient kinetic events that drive transport are difficult to detect (65). Therefore, it is evident that an experimental technique that allows us to directly observe the dynamic nature of the alternating access mechanism is required to definitively prove the alternating access mechanism of these transporters.

1.5. Single-molecule FRET

Single-molecule Förster resonance energy transfer (sm-FRET) offers a powerful biophysical method to measure sensitive changes in transient changes in the conformational dynamics in real-time (65). Förster resonance energy transfer (FRET) occurs as a form of non-radiative energy transfer from an excited donor fluorophore to an acceptor fluorophore to induce detectable levels of acceptor emission to calculate changes of intermolecular distances of a sample between 10-100 Å (66–68). This scale is ideal for measuring subtle changes in distances between chemical moieties in biological macromolecules (69). The efficiency of energy transfer is distance-dependent, where the rate of energy transfer is dependent on the inverse sixth power of distance between the donor and acceptor FRET pair (69). Intermolecular distance between the donor and acceptor (R) can be determined in a biological system provided a measured value regarding total FRET efficiency (E) and known Förster radius (R_0) via the Förster rate equation (66) (equation 1).

$$E=\left(1+\left(\frac{R}{R_0}\right)^6\right)^{-1} \quad \text{(Equation 1)}$$

The integration of single-molecule spectroscopy with the FRET technique has enhanced the power and resolution of FRET towards the analysis of individual, transient-level conformational dynamics to be observed in real-time (70). The application of sm-FRET to study transporters has allowed for the direct observation of distinct transient states of the transporter (65,71–74). The recent advance of the sm-FRET technique to study reconstituted transporters in proteoliposomes has enabled the direct observation of transient kinetics that drive vectorial transport (65,71) (Figure 8A). Hence, sm-FRET offers a viable platform to directly observe the transient kinetics of the proposed alternating access mechanism of multidrug efflux pumps. The study of transient kinetics of the alternating access mechanism of a transporter coupled with direct observation of vectorial transport of a fluorescent substrate can provide the first direct, visual evidence for the alternating access model of transport (Figure 8B).

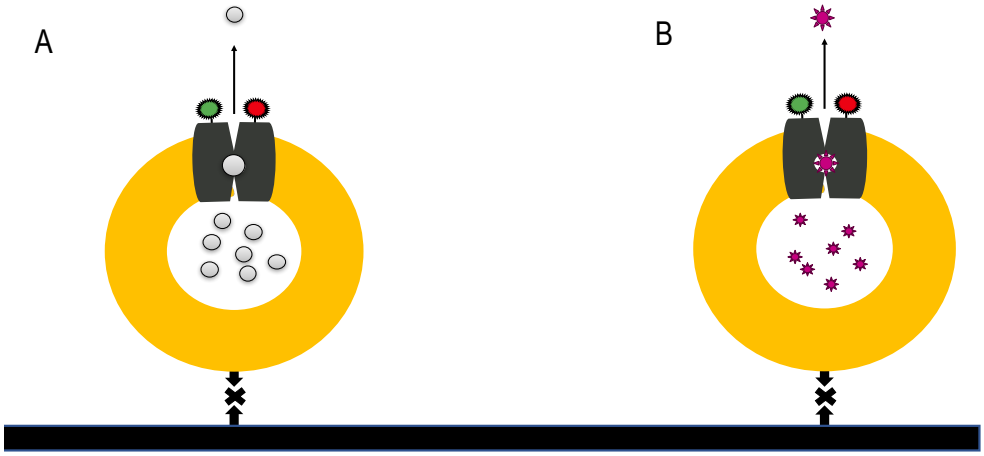

Figure 8. Schematic illustration of a single-molecule FRET transport experiment. A) A transporter (black) is reconstituted into a lipid vesicle (yellow ring) tethered to a microscope slide (black). Concentration gradients can be applied to the liposome and vectorial transport of substrate (grey circles) to be observed as a change in interfluorophore distance can be measured as changes in fluorescence intensity between a donor (green circle) and acceptor (red circle). B) Analysis of vectorial transport of a fluorescent substrate (red stars) coupled to single-molecule FRET can allow for a direct observation of fluorescent substrate transport in parallel with protein domain movement to directly visualise the alternating access model of transport.

1.6. MdfA, a model efflux pump for investigating the alternating access mechanism

MdfA is a well-characterised H^+/drug antiporter the MFS family from *E. coli*, that exhibits the capacity to confer resistance to a diverse range of neutral, zwitterionic and monovalent cationic compounds (75). MdfA acts as a single-component transporter composed of a twelve transmembrane α-helices divided into N-terminal (TM1-6) and C-terminal domains (TM7-12) (76).

Crystallisation of MdfA revealed the two domains are organised into a pseudo two-fold symmetry of three helical repeats that is archetypal of MFS transport protein structure (56). The structure of MdfA is well-characterised, whereby the cavity helices (TM1, TM4, TM7 and TM10) face inward towards the central cavity to generate a hydrophobic binding pocket, that harbours two essential protonatable residues (E26 and D34) critical for binding neutral and cationic compounds (56). The rocker helices (TM2, TM5, TM8 and TM11) are arranged to flank the cavity helices to provide physical occlusion of the substrate-binding site and support conformational change during substrate transport (7,56). Last, the support helices (TM3, TM6, TM8 and TM12) play a role supporting the structural integrity of MdfA (56). Thus, MdfA presents significant structural evidence for a rocker-switch mechanism of alternating access (7,54,56). MdfA exhibits two highly-conserved protonatable residues (E26, D34) embedded within the hydrophobic cavity on TM1. These residues were determined to be critical for electroneutral transport of cationic substrates. However, only one of either of these residues are required for electrogenic transport of neutral compounds (77). It is proposed D34 is the primary protonation site, which supports the 'ping-pong' mechanism of direct competition of substrate and proton within the binding site of MFS antiporters (54,78). However, as neither E26 or D34 are essential for substrate binding, it is proposed that the 'ping-pong' mechanism is likely to be an indirect exchange between substrate and proton mediated by an allosteric effect (79).

The extensive biochemical and structural characterisation MdfA has led to two models of alternating access to be proposed (56,78). In the first mechanism, proposed by Fluman *et al.,* MdfA rests in the inward-facing conformation (78). Transport is initiated upon the deprotonation of D34 on TM1. A proton is released into the cytoplasm by translocating from D34 to E26 (78). Loss of a single proton is proposed to promote substrate binding into the binding cavity of MdfA (78). This event triggers a conformational switch to the outward-facing state to release substrate to the periplasmic face (78). Here, it is only when substrate is released that D34 becomes protonated to trigger a conformational change back into the inward-facing conformation (78). In the second model, it is proposed that MdfA alternatively rests in the outward-facing state of which E26 acts as the primary pronated residue. However, questions are raised as to how a proton is translocated from E26 to D34, 11Å away against an electrochemical gradient to trigger the inward-facing conformation for substrate-loading (Yardeni *et al.,* unpublished).

MdfA has been characterised to transport monovalent cationic substrates and has been associated to confer resistance to a range of fluorescent antimicrobial substrates including ethidium bromide and rhodamine 6G (R6G) (75). R6G is a highly fluorescent substrate ideal for single-molecule fluorescence experiments due to its high quantum yield ($\Phi = 0.95$) and has been frequently used in

single-molecule experiments (80,81). Therefore, MdfA represents an exceptional target that could potentially allow direct single-molecule FRET studies of the alternating access mechanism, while simultaneously observing export of a highly fluorescent substrate, R6G.

1.7. Objective of this study

The long-term goal of this project is to provide the first direct evidence of the alternating access mechanism of a transport protein using single-molecule FRET. To achieve this outcome, it is essential to successfully characterise a model protein to transport a fluorescent substrate suitable for detection using single-molecule fluorescence microscopy. Following this step entails the design of an active derivative of the protein of interest, that will accept site-specific labelling of a FRET pair to directly observe the mechanism of alternating access using single-molecule FRET. A Cys-less (CL) mutant of MdfA, with two introduced cysteines at the apex of the N-terminal domain (V44) and C-terminal domain (V307) on MdfA (MdfA_CL_V44C/V307C) offers an ideal scaffold for site-specific labelling of a FRET pair by a selective cysteine-maleimide dye conjugation reaction. The plasmid encoding this protein was kindly donated the Bibi laboratory group (Weizmann Institute of Science, Israel). The next step is to assess for an activity difference between wild-type and Cys-variant MdfA before site-specific labelling with a FRET pair for an ensemble FRET study of the FRET-labelled MdfA solubilised in detergent using standard fluorometry. The next step is the reconstitution of FRET-labelled protein into proteoliposomes, for direct observation of real-time conformational dynamics of the alternating access mechanism in parallel to simultaneous detection of vectorial substrate movement using a fluorescent substrate. The scope of this project extends beyond the term of a ten month MRes degree. Therefore, the aims of this thesis are dedicated to the first steps required for this project, to reach the goal to directly observe the alternating access mechanism of vectorial transport in an active transporter for the first time.

The following aims to achieve these outcomes are described below.

1) To validate that MdfA mediates direct R6G transport.
2) To successfully purify MdfA for functional characterisation.
3) To confirm MdfA directly binds R6G.
4) To assess the activity of a Cys-variant of MdfA.
5) To develop a novel fluorescence transport assay to detect real-time transport of R6G in single *E. coli* cells overexpressing the Cys-variant MdfA.

Chapter 2. Materials and Methods

2.1. General chemicals

All chemicals and reagents used throughout this thesis were purchased by Sigma-Aldrich unless otherwise specified in Table 1. All buffers, stocks and working solutions were prepared in filter sterilised ddH_20 unless otherwise specified.

Table 1. List of Chemicals and Reagents

AMRESCO, USA	Glycerol HEPES free acid *L*-tryptophan
Astral Scientific, Australia	Ampicillin Sodium Salt Kanamycin Sulphate
Avanti Polar Lipids, USA	n-dodecyl-ß-D-maltoside (DDM)
Alfa Aesar, USA	6X Laemelli SDS-Loading Dye
Bacto, Australia	BD Difco™ Luria-Bertani broth, Miller BD Difco™ Mueller-Hinton broth
Biochemicals, Australia	Potassium phosphate, dibasic Potassium phosphate, monobasic tris(hydroxymethyl)aminomethane (TRIS) base
Chem-Supply, Australia	Ethanol
Dow Corning, Australia	SYLGARD® 184 Silicone Elastomer Kit
GE Healthcare Life Sciences, USA	Amersham ECL High-Range Rainbow Molecular Weight Marker
Panreac, Germany	Glacial Acetic Acid
Takara Bio, USA	SOC media
Teknova, USA	EZ Rich Defined Media
Thermo Scientific, Australia	Coomassie Brilliant Blue R-250 Dye HisProbe™ -HRP Conjugate HisPur™ Cobalt Resin Tween™ 20 Surfact-Amps™ Detergent Solution
VWR International	Glycine

2.2. Bacterial strains

Three *E. coli* strains were used throughout this work. *E. coli* DH5α (Alpha-Gold Select, Bioline) was used as a host for plasmid preparations and as a non-arabinose metabolising host for live cell efflux assays. The *E. coli* UTL2*mdfA::kan* strain was used throughout this work to express, purify and assess the function of overexpressed native MdfA and MdfA_CL_V44C/V307C in the absence of the native MdfA protein that is encoded in the chromosome of *E. coli*. Strain, genotype and source of strains are described in Table 2.

Table 2. *E. coli* strains and mutants

***E. coli* Strain**	**Genotype**	**Source**
DH5α	*F^- deoR endA1 recA1 relA1 gyrA96 hsdR17(rk^-, mk^+) supE44 thi^{-1} phoA Δ (lacZYA argF) U169 Φ 80lacZ Δ M15λ $^-$*	Bioline
UTL2*mdfA::kan*	*F- ara-14 leuB6 secA6 lacY1 proC14 tsx-67 Δ(ompT-fepC)266 entA403 trpE38 rfbD1 rpsL109 xyl-5 mtl-1 thi-1 mdfA::kan*	(82)

2.3. Plasmids

Plasmids used throughout this work were kindly gifted by the Bibi group from the Weizmann Institute of Science (Rehavot, Israel). Plasmids are described in Table 3.

Table 3. Plasmids

Plasmid	**Description**	**Selection**
pUC18/pAra/mdfA	pUC18 expression vector encoding wild-type MdfA(6His) behind the pAra promotor.	Ampicillin
pUC19/pBAD/mdfA_CL_V44C/V307C	pUC19 expression vector encoding MdfA_CL_V44C/V307C(6His) behind the pBAD promotor	Ampicillin

2.4. Microbial culture conditions

E. coli strains were routinely grown in Luria-Bertani (LB) broth (10 g/L NaCl, 5 g/L yeast extract and 10 g/L tryptone) at 37°C, shaking (200 rpm). For plasmid selection, media was supplemented with 100 μg/mL ampicillin unless stated otherwise. All microbial culture media used for *E. coli* cell culture were prepared in MilliQ water and sterilised by autoclaving.

2.5. Preparation of chemically competent *E. coli* cells

E. coli cells stored in 20% glycerol stocks at -80°C were streaked onto a non-selective LB agar plate. A single bacterial colony was inoculated into 10 mL of fresh LB media without antibiotic and incubated for 16 hrs overnight at 37°C, shaking (200 rpm). The starter culture was sub-cultured into 800 mL of fresh LB media at a 1:125 dilution and grown to an optical density at 600 nm (OD_{600}) of 0.35-0.4. The cell culture was chilled on ice for 30 minutes and the cells harvested by centrifugation (3000 x *g*, 15 min, 4°C). Supernatant was removed and the cell pellet was gently resuspended in 20 mL of cold 100 mM $MgCl_2$. Cells were harvested by centrifugation (2000 x *g*, 15 min, 4°C). The cell pellet was resuspended in 40 mL of ice cold 100 mM $CaCl_2$ and chilled on ice for a further 20 minutes prior to cell harvest (2000 x *g*, 15 min, 4°C). The cell pellet was resuspended in 20 mL of chilled 85 mM $CaCl_2$ containing 15% glycerol. The cells were harvested by centrifugation (1000 x *g*, 15 min, 4°C) and resuspended in 2 mL of 85 mM $CaCl_2$ containing 15% glycerol. Cell samples were aliquoted into 50 µL fractions into pre-chilled sterile 1.5 mL microfuge tubes and stored at -80°C.

2.6. Transformation of chemically competent cells

For transformation of *E. coli* strains, 10 µL of chemically competent *E. coli* cells were incubated with 1 µL of plasmid for 30 minutes on ice. Cells were heat-shocked at 42°C for 40 seconds in a water-bath followed by an immediate incubation on ice for 2 minutes. For recovery, 950 µL of SOC media was added to the cells for incubation at 37°C at 200 rpm for 1 hour. Cells were plated onto LB-agar plates with 100-200 µg/mL ampicillin for plasmid selection and incubated for 16 hours at 37°C. Plates were then sealed with parafilm and stored at 4°C for one month.

2.7. Plasmid extraction and quantitation

Plasmid preparations were routinely performed on *E. coli* cells harbouring the plasmid of interest using the Wizard® Plus SV Miniprep DNA purification system (Promega, USA) according to the manufacturer's instructions. Plasmid concentrations were determined using a NanoDrop 1000 (Thermo Scientific, USA) by measuring the absorbance at 260 nm, and checked for purity by determining the ratio of absorbance at 260/280 nm (ratios of ≥1.8 were seen as acceptable). Plasmid DNA isolated using this method was used for subsequent transformation of chemically competent *E. coli* strains.

2.8. Minimum inhibitory concentration assays

MdfA-mediated resistance to R6G in *E. coli* cells was tested using a broth microdilution minimum inhibitory concentration (MIC) technique as described (83). Single colonies of *E. coli* strains were inoculated in 5 mL of Mueller-Hinton (MH) broth and supplemented with appropriate antibiotics for

plasmid selection if required. Cultures were grown for 16 hours overnight at 37°C, shaking (200 rpm). Stocks of R6G were prepared in methanol (stored at 4°C for up to 2 months). Two-fold serial dilutions of antimicrobial from these concentrations were performed across a 96-well microtiter plate (Grenier Bio-One, Austria) to achieve geometrically decreasing concentrations of the substrate of interest starting from column 1 to column 10. Column 11 was reserved as a positive control to test for bacterial growth and column 12 is reserved as a negative control to assess sterility of the media. For the R6G assays, the highest concentration tested was 500 μg/mL (column 1) and lowest concentration was 0.9 μg/mL (column 10). To prepare culture for MIC assays, overnight cultures were sub-cultured to a final dilution of 1:50 in MH broth in the absence of antibiotic and grown to an OD_{600} = 0.6 at 37°C with shaking at 200 rpm. Cells were diluted 1:11,000 and plated into the positive control wells and across wells containing the compound of interest from least concentrated to most concentrated to avoid compromising substrate concentrations from cross-contamination. MIC plates were incubated for 24 hours at 37°C, shaking (200 rpm). At 24 hours, OD_{600} was measured across each well using a PHERAstar FS (BMG LABTECH, Germany). The MIC was determined as the lowest concentration at which bacterial growth was inhibited. R6G inhibition assays were performed accordingly with the exception that inhibition assays were all performed with the use of LB broth as a growth medium in substitute of MH broth.

2.9. Fluorometric transport assays

Single colonies of freshly transformed *E. coli* strain UTL2*mdfA::kan* harbouring the pUC18/pAra/mdfA or pUC19/pBAD/mdfA_CL_V44C/V307C plasmids were inoculated into 10 mL of fresh LB broth supplemented with 200 μg/mL ampicillin and 30 μg/mL kanamycin for overnight culture at 37°C with 200 rpm shaking. Overnight cultures were sub-cultured following a 1:10 dilution into fresh sterile LB with supplemented with 100 μg/mL ampicillin, 30 μg/mL kanamycin and grown to OD_{600} = 0.8. A pre-induction sample was reserved and MdfA overexpression in the remaining cultures was induced with L-arabinose at 10x fold increases in concentration (0.2%, 0.02%, 0.002% or 0.0002%) to assess the impact of the MdfA expression level on the ethidium bromide transport phenotype. R6G fluorometric transport assays were conducted at the 0.002% v/v L-arabinose induction condition. Samples were overexpressed for 1 hr at 37°C at 200 rpm. Cells were harvested by centrifugation (4,500 x *g*, 3 minutes) and washed twice by sequential resuspension in 10 mL of assay buffer (20 mM KOH-adjusted HEPES buffer, pH 7.0) and harvested by centrifugation (4,500 *x g* for 3 minutes). Cells were resuspended to OD_{600}=1.0 in assay buffer and divided into 1 mL aliquots for treatment with 10 μM carbonyl cyanide 3-chlorophenylhydrazone (CCCP) and 15 μM ethidium bromide or 1 μM R6G. Cells were incubated at 37°C for 1 hour to facilitate passive diffusion of fluorescent dye into the de-energised *E. coli* cells. Dye-loaded cells were harvested by

centrifugation (4,500 x g, 3 minutes) and subsequently washed twice in assay buffer to remove excess dye and CCCP. Cells were resuspended in assay buffer immediately prior to the transport assay. All transport assays were performed on a LS-55 fluorescence spectrometer (PerkinElmer, USA) using 10 mm x 10 mm disposable polystyrene fluorometer cells (Starna, USA). Fluorometric transport assays were performed at a constant temperature of 37°C maintained using a Julabo HE water circulator (Julabo, USA). Excitation and emission wavelengths were set at 530/610 nm for EtBr and 529/553 nm for R6G with slit widths set at 10 nm and 4.5 nm, respectively. Fluorescence was monitored for ~60 seconds before efflux was initiated by the introduction of 0.5 M sodium formate. Transport was monitored for ~300 seconds before inhibition with 20 μM CCCP to confirm that the changes in fluorescence related to transport were energy dependent, as would be expected for the secondary active transporter MdfA.

2.10. Single cell transport assay

E. coli DH5α harbouring the pUC19/pBAD/mdfA_CL_V44C/V307C plasmid were grown in 500 μL EZ rich defined medium, supplemented with 10% glycerol and 100 μg/mL ampicillin. Cultures were grown overnight at 37°C, shaking (200 rpm). Overnight cultures were sub-cultured 1:100 into 5 mL of EZ rich media supplemented with 10% glycerol supplemented with 100 μg/mL ampicillin and grown to an $OD_{600} = 0.6$ at 37°C, shaking (200 rpm). Cultures were split to yield a non-induced control supplemented with 0.2% D-glucose to suppress MdfA_CL_V44C/V307C overexpression and induced cultures were supplemented with 0.2% v/v L-arabinose to initiate MdfA_CL_V44C/V307C overexpression for 1 hour. Cells were harvested by centrifugation (4,500 x *g*, 10 min) and washed twice in assay buffer (20 mM KOH-HEPES, pH 7.0) before treatment with 10 μM CCCP and 100 μM R6G. Treated cells were incubated for 1 hour at 37°C to facilitate passive diffusion of R6G dye into de-energised *E. coli* cells. Cells were washed three times in assay buffer by repeated cell wash and harvested by centrifugation at 4,500 x g (1 minute) before final resuspension in 1 mL of assay buffer.

Microfluidic polydimethylsiloxane (PDMS) flow cells with channel dimensions of 30 mm x 0.1 mm x 0.5 mm (length x height x width) were fabricated at the Australian National Fabrication Facility (South Australian Node). PDMS flow cells were further modified to allow for sample inlet and outlet points in each flow channel manually using a 3-mm tissue cutter to remove 3x3 mm circular sections of PDMS to generate ~20 μL sample reservoir on either end of the flow channel to facilitate sample introduction and removal. A published method by Robinson *et al.,* 2014 was adapted to prepare the PDMS-based flow cell for a live single-cell efflux assay (84). Briefly, glass coverslips were activated by sonication in 5M KOH for 60 minutes, followed by a thorough rinse with water before incubation

with 2% solution of 3-aminopropyltriethoxysilane (APTES) for 2h. APTES-treated coverslips were washed with acetone and dried. PDMS flow cells was washed thoroughly with ethanol and dried immediately before permanent bonding with APTES-modified coverslips by activation of PDMS using an oxygen plasma cleaner (Zapto, Diener Electronic, Germany).

To prepare samples for imaging, 20 μL aliquots of cell sample were introduced at sample inlets at both ends of the flow channel to saturate the channel with cells. PDMS flow cells were left to incubate for one minute to promote cell adhesion to the APTES-modified coverslips, before aspirating excess sample solution for single-cell imaging. Imaging was carried out on an in-house custom-built wide-field single-molecule fluorescence microscope. The custom-built microscope was based on an inverted fluorescence microscope body (IX-81, Olympus, Japan) equipped with a 1.49 NA 100x objective and 512x512-pixel EM-CCD camera (C9100-13, Hamamatsu, Japan). To image real-time efflux of R6G, the PDMS flow cell containing immobilised *E. coli* cells was excited at 514 nm wavelength at low power (20 $W.cm^{-2}$) using a continuous-wave optically pumped semidiode laser at 514 nm (150 mW max. output, Sapphire LP, Coherent, USA) and emission was collected between 525-555 nm (ET 540/30m filter, Chroma, USA).

Image acquisition was set to an exposure time of 98 milliseconds with image capture 600 x 100 milliseconds using xcellence imaging software (Olympus, Japan). To conduct the live cell efflux assay, non-adherent cells were removed by an assay buffer wash. The washing step was imaged as a control to monitor whether leaky efflux of R6G was present before initiation of the single-cell transport assay. To visualise energy-dependent efflux of R6G, assay buffer supplemented with 0.5M sodium formate was introduced to the flow channel to re-energise cells to observe direct R6G efflux mediated by cells overexpressing MdfA_CL_V44C/V307C. This experiment was performed across three biological replicates against MdfA_CL_V44C/V307C overexpressing cells and a pre-induction sample as a control. Images were processed using ImageJ software (85).

2.11. Microbial growth curves

Single colonies of *E. coli* strain UTL2*mdfA::kan* cells and transformants harbouring either pUC18/pAra/mdfA plasmid for WT MdfA overexpression and pUC19/pBAD/mdfA_CL V44C/V307C were grown in sterile Luria-Bertani (LB) media containing kanamycin (30 μg/mL) and further supplemented with ampicillin (200 μg/mL) for plasmid selection during overnight culture at 37°C at 200 rpm. Overnight cultures were sub-cultured 1:50 in fresh LB broth supplemented with 30 μg/mL kanamycin and 100 μg/mL ampicillin for plasmid selection and grown to mid-log phase (OD_{600} = 0.5-0.6). Samples were treated with 10x increasing concentrations of L-arabinose inducer

(0.2%, 0.02%, 0.002%, 0.0002%) and plated across a 96-well plate for high-throughput screening of growth curves over 5 hours to determine ideal L-arabinose growth conditions.

2.12. Scanning electron microscopy

E. coli UTL2*mdfA::kan* cells harbouring the pUC19/pBAD/mdfA_CL_V44C/V307C plasmid were grown in overnight culture in 5 mL of LB broth supplemented with 200 μg/mL ampicillin and 30 μg/mL kanamycin. Culture was incubated for 16 hours at 37°C, shaking (200 rpm). The overnight culture was sub-cultured into a final dilution of 1:50 into 12.5 mL of fresh LB broth supplemented with 100 μg/mL ampicillin and 30 μg/mL kanamycin and grown at 37°C at 200 rpm to a final OD_{600} = 0.8. A 2 mL pre-induction sample was collected before inducing cells with 0.2, 0.002 or 0.0002% v/v L-arabinose. The cultures were incubated for a further hour at 37°C at 200 rpm to facilitate overexpression of MdfA_CL_V44C/V307C. Culture samples were dispensed in 50 μL aliquots onto sterile, 12 mm round coverslips (ProSciTech, Australia) derivatised with 0.1% poly-L-lysine to facilitate *E. coli* adhesion to the coverslip before fixation. After 1 minute, excess solution was aspirated and a second 50 μL aliquot of culture was applied to the coverslip for another minute. To fix cells, coverslips were washed twice with phosphate buffered saline (PBS) and were transferred to a sterile 6-well plate containing 2 mL of 3% glutaraldehyde in sterile 0.01 M phosphate buffered saline (PBS). Cells were fixed for 24 hours at 4°C. Fixed cells were washed twice in 2 mL of sterile 0.01 M PBS for 2 minutes and excess PBS solution was aspirated. To dehydrate cells for SEM imaging, a sequential ethanol dehydration step was performed by washing each coverslip in 30% v/v, 50% v/v, 70% v/v, 80% v/v, 90% v/v and twice with 100% anhydrous ethanol for 10 minutes. Samples were subject to critical point drying using a Leica EM CPD300 (Leica, Germany) for 2 hours. Samples were desiccated overnight and sputter coated in gold (EMITECH K550X Sputter Coater, Quorum Technologies, UK) before SEM image acquisition using a JSM-6480LA scanning electron microscope (JEOL, Japan) at an accelerating voltage of 10 kV. Unequal variance *t*-tests were used to evaluate statistical significance between average length of *E. coli* cells at different L-arabinose growth conditions.

2.13. Purification of MdfA

Wild-type MdfA and MdfA_CL_V44C/V307C were purified from a method adapted from Fluman *et al*., 2014 (86). All sample handling steps throughout the purification procedure were performed at 4°C unless stated otherwise. Buffers used in the protein purification protocol are listed in Table 4.

Table 4. List of buffers and their chemical components used throughout purification.

Buffer	Chemical components
Cell wash buffer	50 mM potassium phosphate (pH 7.3), 2 mM $MgSO_4$
Solubilisation buffer	20 mM Tris-HCl (pH 8.0), 500 mM NaCl, 10% glycerol, 5 mM imidazole, 3.5 mM β-mercaptoethanol.
Wash buffer	20 mM Tris-HCl, (pH 8.0), 500 mM NaCl, 10% glycerol, 5 mM imidazole, 0.1% DDM
Elution buffer	20 mM Tris-HCl, (pH 7.2), 120 mM NaCl, 10% glycerol, 150 mM imidazole, 0.1% DDM
Desalting buffer	20 mM Tris-HCl, pH (7.2), 120 mM NaCl, 10% glycerol, 0.01% DDM

2.13.1. Overexpression of MdfA

Chemically competent *E. coli* UTL2*mdfA*::*kan* cells were transformed with the plasmid pUC18/pAra/mdfA or with the plasmid pUC19/pBAD/mdfA_CL_V44C/V307C. Transformation samples were plated on LB-agar plates supplemented with 200 μg/mL ampicillin and incubated for 16 hours overnight at 37°C. Successful transformants were inoculated into 5 mL of sterile LB broth supplemented with 200 μg/mL ampicillin and 30 μg/mL kanamycin for plasmid selection and grown overnight for 16 hours at 37°C, shaking (200 rpm). To express wild-type MdfA and MdfA_CL_V44C/V307C to a level sufficient for purification, cells were inoculated into 6 x 2L flasks containing 500 mL sterile LB media supplemented with 100 μg/mL ampicillin and 30 μg/mL kanamycin. The overnight cultures were sub-cultured into these flasks by diluting 1:100 and incubated in a flat-bed shaker at 37°C at 200 rpm to grow until OD_{600} = 0.8-1.0 was reached. Subsequent protein expression was induced upon the addition of 0.2% v/v L-arabinose and incubation was continued at 16°C with shaking at 200 rpm for 16 hours overnight. Induced cells were harvested by centrifugation (6,000 x *g*, 30 minutes) and washed with cell wash buffer. Washed cells were collected by centrifugation (6,000 x g, 30 minutes) and resuspended in cell wash buffer prior to storage at -80°C.

2.13.2. Membrane extraction

Thawed cell suspensions were treated with 1 mM PMSF solubilised in methanol and 10 μg/mL DNase I prior to cell lysis by the French Pressure method. Samples were subjected to three passages

of French Press method at 15,000 psi (French® Press, Thermo IEC, USA) and cooled on ice between each passage to reduce overheating of samples. Insoluble cell debris was removed by centrifugation (5,000 x *g*, 15 minutes) followed by collection of the membrane fraction by ultracentrifugation (167,000 x *g*, 1 hour). Membrane fractions were homogenised in a Dounce homogeniser in solubilisation buffer (8 mL per gram) and stored at -80°C.

2.13.3. Co^{2+} affinity purification of MdfA

To isolate pure MdfA from membrane extracts, thawed membrane fractions were treated with 1.1% DDM and incubated at 4°C with continuous stirring for 2 hours. Residual insoluble debris was removed by ultracentrifugation (167,000 x *g*, 1 hour). Co^{2+} resin (HisPur™ Cobalt Resin, Thermo Scientific, USA) was equilibrated in loading buffer, prior to the addition of supernatant for incubation at 4°C for 2 hours to promote protein binding to the column before transfer to a disposable gravity-flow column to facilitate immobilised metal affinity chromatography (IMAC) to isolate MdfA. Upon transfer, flow-through was immediately discarded and the column was washed with 30 column volumes of loading buffer to remove weakly-associating proteins. To elute MdfA, 1 column volume of elution buffer was incubated with cobalt resin for 10 minutes before collecting each fraction. Elution fractions were monitored throughout by monitoring absorbance at A_{280} (NanoDrop 1000, Thermo Scientific, USA). The concentration of protein was calculated via the Beer-Lambert law using absorption at 280 nm and the molar extinction coefficient of MdfA (ε = 70510) and MdfA_CL_V44C/V307C (ε = 69900) were predicted by the ProtParam program (87).

2.14. Buffer exchange

Chromatography fractions deemed to containing sufficient concentrations of protein were subject to buffer exchange to remove smaller molecules before functional characterisation (such as imidazole). Two buffer-exchange methods of were assessed to identify the optimal method to recover the highest level of MdfA post-purification.

2.14.1. Spin-column

The buffer exchange method was trialled using PD-10 disposable desalting columns (Amersham Biosciences, USA) according to the manufacturer's protocol. PD-10 desalting column was prepped by removal of column storage solution and filter using sterile forceps. Column seal was removed and column was transferred to a 50mL falcon tube with a respective column adapter. To equilibrate the column for buffer exchange, the column was filled with desalting buffer and allowed to enter the packed bed. This was repeated thrice and flow-through was discarded each time. The fifth equilibration was centrifuged (1000 x *g* for 2 minutes) and the flow-through was discarded. Protein

eluate was applied and allowed to enter the packed bed and column was transferred to a fresh 50 mL falcon tube to collect desalted protein sample by centrifugation (1000 x g, 2 minutes). Sample concentration was analysed by the A_{280} method (NanoDrop 1000, Thermo Scientific, USA). Samples were concentrated to ~1 mg/mL (Vivaspin® 20,10 kDa MWCO, GE Healthcare, USA). For storage, concentrated sample was divided into 50 µL aliquots, snap frozen in liquid N_2 and stored at -80°C.

2.14.2. Gravity-flow

PD-10 desalting column was prepared for gravity-flow buffer exchange of protein eluate by removal of column storage solution and equilibration against 25 mL total desalting buffer. A total of 2.5 mL of protein sample was applied to the column and allowed to enter the packed bed. Flow through was discarded and the column was transferred to a fresh 50 mL falcon tube to collect desalted protein eluate. A total of 3.5 mL of desalting buffer and 2.5 mL of protein eluate was collected. The final protein concentration was analysed by A_{280} (NanoDrop 1000, Thermo Scientific, USA) and concentrated to ~1 mg/mL (Vivaspin® 20,10 kDa MWCO, GE Healthcare, USA). For storage, sample was divided into 50 µL aliquots, snap-frozen in liquid N_2 and stored at -80°C.

2.15. Qualitative analysis of protein purification

2.15.1. Sodium dodecyl sulphate-polyacrylamide gel electrophoresis (SDS-PAGE)

SDS-PAGE was routinely performed to assess expression levels and purity of MdfA throughout the purification procedure as described in section 2.13. Small samples (40 µL) were collected throughout the purification procedure and were incubated in a 1:1 ratio with 6x Laemmli reducing SDS sample buffer (375 mM Tris-HCl pH 6.8, 9% SDS, 50% glycerol, 9% β-mercaptoethanol, 0.03% bromophenol blue) at 37°C for 20 minutes. Samples were loaded onto pre-cast 4-20% tris-glycine polyacrylamide gels (4–20% Mini-PROTEAN® TGX™ Precast Protein Gels, Bio-Rad, Australia) and electrophoresed in parallel with a molecular weight standard (Amersham ECL High-Range Rainbow Molecular Weight Marker, GE Healthcare Life Sciences, USA). Gels were run in 1X SDS running buffer (25 mM Tris-HCl, 250 mM glycine, 10% w/v SDS). Gel electrophoresis was run at 110 V for 1 hr and 30 minutes. Gels were fixed for 10 minutes in fixer (10% v/v acetic acid, 50% v/v ethanol), followed by staining for 5 minutes with Coomassie stain solution (0.25% w/v Coomassie brilliant blue, 10% v/v ethanol, 10% v/v acetic acid), followed by overnight destain with destain solution (10% v/v acetic acid). Gels were imaged using the Gel Logic 2200 pro imaging system (Carestream Health, USA) set to capture images under the white-light trans-illumination setting.

2.15.2. Western blot

Western blots were used to verify the expression and isolation of His-tagged MdfA protein after purification. Samples of interest were separated by SDS-gel electrophoresis followed by a brief wash for 10 minutes with Towbin buffer (25 mM Tris pH 8.3, 192 mM glycine, 20% v/v methanol). Polyvinylidene fluoride (PVDF) membrane was activated in methanol for 1 minute, followed by rinsing in water for 5 minutes and final incubation in Towbin buffer for 10 minutes. To allow for protein transfer from the SDS-PAGE gel to the PVDF membrane via the semi-dry electroblotting transfer method, a semi-dry transfer stack was prepared. The semi-dry transfer stack was comprised of five sheets of Whatman filter paper, pre-soaked with Towbin buffer, followed by the activated PVDF membrane, the SDS-PAGE gel and an additional five sheets of Whatman filter paper, pre-soaked with Towbin buffer. Excess buffer was drained and air-bubbles were removed before semi-dry transfer was conducted at 10 V for 1.4 hours using the Novex™ Semi-Dry Blotter (Invitrogen, USA). Post-transfer, PVDF membrane was washed twice with TBS buffer (25 mM Tris, 0.15 M NaCl, pH 7.2) for 10 minutes, with gentle shaking (<50 rpm). Membrane was blocked with 10 mg/mL BSA in TBST (25 mM Tris, 0.15 M NaCl, 0.05% Tween-20, pH 7.6) overnight at 4°C, shaking. The PVDF membrane was washed twice with TBST for 10 minutes. To probe His-tagged proteins, the membrane was incubated 1:5000 dilution of HisProbe-HRP™ (Thermo Scientific, USA) in TBST for 1 hour with gentle shaking at room temperature. The membrane was washed four times with TBST for 10 minutes each. For chemiluminescent detection, membrane was incubated in SuperSignal™ West Pico Substrate Working Solution (Thermo Scientific, USA) for 5 minutes, with shaking, in the dark and subsequently imaged with the Gel Logic 2200 Pro in progressive mode, with 2 to 5 minute exposure time under the luminescence setting.

2.16. Tryptophan fluorescence quenching assay

Tryptophan fluorescence quenching measurements were performed on a PerkinElmer LS55 fluorescence spectrophotometer at a constant temperature of 25°C using a heating water-circulator (Julabo HE, Germany). To prepare R6G for titration, a 10 mM R6G stock solution was prepared in methanol and subject to a 10x fold serial dilution in assay buffer (20 mM Tris-HCl, pH 7.2, 120 mM NaCl, 10% glycerol, 0.01% DDM) to achieve working concentrations of 1 mM, 0.1 mM and 0.01 mM of R6G in buffer for tryptophan quenching experiments. MdfA protein samples were diluted to a final concentration of 1 μM in 150 μL of buffer in a 10 mm x 10 mm Quartz Suprasil® cuvette (PerkinElmer). Tryptophan residues (n= 10) were selectively excited at 295 nm and fluorescent emission was monitored between 300-450 nm. R6G was titrated in aliquots of 0.7-3.7 μL aliquots against increasing concentrations of R6G (0.01 mM, 0.1 mM, 1 mM) in buffer. All readings were

corrected for background emission of the buffer and sample dilution. Inner filter effect was accounted for by titrating against 1 μM of pure tryptophan in a parallel tryptophan quenching experiment.

Corrected fluorescence quenching values for MdfA titrated against R6G was determined by equation 1:

$$\Delta F_C = \frac{\Delta F_P - F_{Pi}\left(\Delta F_w / F_{Wi}\right)}{F_{Pi}} \qquad (1)$$

where ΔF_C represents the corrected fluorescence quenching value, ΔF_P= the reduction in MdfA Trp fluorescence at a certain concentration of ligand, F_{Pi} = initial fluorescence of MdfA, ΔF_w = reduction in free tryptophan fluorescence intensity at a certain concentration of ligand and F_{Wi} = the initial fluorescence intensity of free tryptophan. The dissociation constant (K_d) was extrapolated from a plot of plot of 1/[R6G] against $1/\Delta F_C$, using curve-fitting program Kaleidagraph (Synergy Software) against equation 2.

$$y=[M1] \times \frac{[M0]}{[M2][M0]} \quad (2)$$

Where M1 represents total unbound [R6G] concentration, M0 represents total [R6G] concentration, M2 represents the determined K_D value.

Chapter 3. Characterisation of MdfA mediated efflux of R6G

MdfA is a well-characterised multidrug efflux pump. As such, it offers a unique model for single-molecule FRET studies due to significant evidence for an alternating access transport mechanism. MdfA has a proposed capacity to efflux a broad range of fluorescent substrates that could be used to observe transport of the fluorescent substrate. However, whether MdfA is capable of direct binding and transport of the highly fluorescent compound rhodamine 6G has not been conclusively shown. This chapter investigates the capacity for MdfA to transport and bind R6G using an ensemble of spectrofluorometric techniques. Together, these results provide a significant step forward to evaluating whether MdfA be viable as a model efflux pump for real-time studies of alternating access at the single-molecule level coupled with direct observation of rhodamine 6G transport.

3.1. Rhodamine 6G resistance assay

Minimum inhibitory concentration (MIC) assays are often used as an initial screen to assess activity of multidrug efflux pumps in reducing the susceptibility of bacteria against antimicrobial agents. This is often determined by performing a broth-microdilution assay to determine the lowest concentration of antimicrobial required to inhibit bacterial growth (83). Therefore, this method was investigated to assess whether overexpression of MdfA from an arabinose inducible expression system could confer heightened resistance to R6G (section 2.8). In MH medium, the MIC showed no bacterial growth across all sample types after 24 hours. To account for potential sub-optimal growth of *E. coli* UTL2*mdfA::kan* cells in cation-adjusted MH-broth, R6G resistance assays were assessed in LB-media (section 2.8). Growth was measured across all samples to determine whether MdfA overexpression conferred improved resistance to R6G (Table 5). LB-resistance assays revealed MdfA_CL_V44C/V307C was inhibited at 500 μg/mL of R6G, whereas both the parental control and wild-type MdfA expression cells demonstrated resistance >500 μg/mL.

Table 5. R6G resistance assays against MdfA overexpressing *E. coli* UTL2*mdfA::kan* cells

	Inhibitory concentration of R6G (μg/mL)		
Media	Control	pUC18_MdfA	pUC19_MdfA_CL_V44C/V307C
MH broth	-	-	-
LB broth	>500	**>**500	500

These results reveal that there is too a high a level of background resistance to observe any MdfA-mediated resistance to R6G in *E. coli* UTL2*mdfA::kan* cells. Therefore, this assay was inconclusive

for demonstrating MdfA-mediated resistance to R6G. Previous work by Edgar & Bibi demonstrate MdfA confers slight resistance to R6G in *E. coli* HB101 cells overexpressing MdfA under T7 RNA polymerase control using the pT7-5(*mdfA)* plasmid in an LB-broth resistance assay (77).

The inconclusive nature of the R6G resistance assay in this study could be due to factors such as the permeability barrier of the outer membrane, or potentially weak antimicrobial activity of R6G towards *E. coli*. Alternatively, a study by Tal & Schuldiner on three major multidrug efflux pumps in *E. coli* – AcrAB (RND), EmrE (SMR) and MdfA (MFS) discovered that individual knockouts of single-component pumps EmrE and MdfA did not affect resistance profile of *E. coli*. However, a double knockout of genes encoding single-component multidrug efflux pumps EmrE and MdfA demonstrated a substantial increase in cell susceptibility to toxic dyes acriflavine and ethidium bromide to a similar susceptibility of a single knockout genes encoding the major RND efflux pump AcrAB (88). This suggests a synergistic nature of single component inner-membrane efflux pumps, such as MdfA to extrude noxious compounds from the cytoplasm to the periplasm, with tripartite RND efflux pump AcrAB-TolC system. Furthermore, an investigation led by Nishino and Yamaguchi revealed no change in the R6G resistance profile of *E. coli* KAM3 cells and *E. coli* KAM3 cells overexpressing MdfA in a pUC118(*mdfA*) plasmid under the regulation of an endogenous promotor (89). However, considerable resistance to R6G was only observable following the overexpression of four distinct tripartite efflux complexes: MFS member- EmrAB-TolC and RND members – AcrAB, AcrEF and YhiUV (89). This data provides evidence that MdfA presence or absence may not have an impact on the resistance profile against of *E. coli* against R6G, possibly due to the synergistic role in R6G efflux with major tripartite complexes that may perform significant R6G efflux across the double-membrane of the Gram-negative cell. Higher concentrations of R6G were not investigated due to pigmentation of R6G that may obstruct absorbance readings at OD_{600}. Additionally, lowered susceptibility to R6G demonstrated by MdfA_CL_V44C/V307C may suggest that the amino acid modifications to generate a MdfA model for FRET studies may demonstrate hindered transport activity compared to wild-type MdfA, which may have hampered cell viability and subsequent resistance threshold against R6G (see section 4.4).

In this study, the R6G resistance assays were tested as a quick initial screen for a multidrug efflux pump to confer resistance against R6G. The inconclusive data indicates that the resistance assays did not demonstrate sufficient sensitivity to conclusively demonstrate whether R6G is a substrate of MdfA. Therefore, further experimentation was required to confirm whether MdfA has potential to bind and transport R6G.

3.2. Rhodamine 6G fluorometric transport assays

An examination of the putative role of MdfA in direct R6G efflux would benefit from a real-time fluorometric transport assay. In principle, a fluorometric assay on multidrug efflux pumps can be carried out by initially de-energising the cells overexpressing the efflux pump of interest by treatment with an energy-decoupling agent, such as carbonyl cyanide *m*-chlorophenylhydrazone (CCCP) that decouples the proton gradient, and hence inhibits secondary active transporters (14). In the presence of these compounds, cells can be loaded with fluorescent amphiphilic or hydrophobic dyes that can passively diffuse into the cell. Dye-loaded cells can be washed multiple times to ensure no trace inhibitor or external dye remains. Initial fluorescence is measured before re-energisation with a metabolite, commonly D-glucose or sodium formate to initiate the efflux by energy-dependent multidrug efflux pumps, where real-time transport is detected as an observable change in detected fluorescence intensity as the fluorophore is exported out of the cell (14). Fluorescent antimicrobial compounds acriflavine and ethidium bromide are well-suited to fluorometric transport assays as a change in fluorescence intensity as substrate is transported across the cell is significant (14).

R6G is known to bind to DNA (90,91). However, it is unknown whether R6G may quench or fluoresce brightly upon binding to DNA. This feature is important as it would determine whether R6G fluorescence may increase or decrease over time as a function of direct R6G export out of the *E. coli* cells overexpressing MdfA. To determine if R6G is suitable to conduct a whole-cell fluorescence transport assay, an initial experiment was conducted by adding a final concentration of 10 µg/mL of dsDNA to 1 µM of R6G in 20 mM HEPES (pH 7.0). This experiment was performed in triplicate and revealed consistent quenching activity of R6G up to ~37% initial fluorescence of R6G with minimal error (Figure 9). Therefore, a R6G whole-cell transport assay against *E. coli* overexpressing MdfA was determined to be practicable.

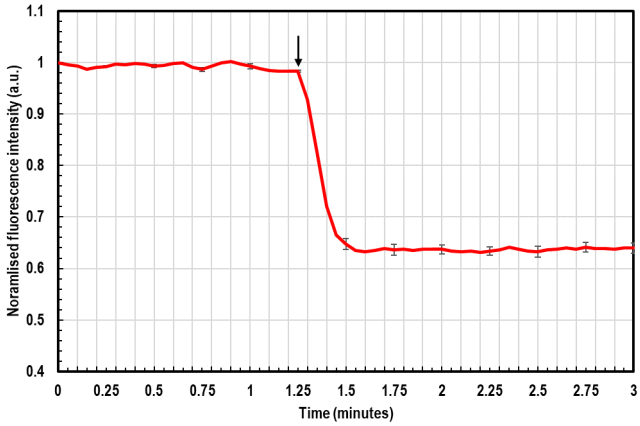

Figure 9. Rhodamine 6G DNA quench assay. R6G (1 µM) against 10 µg/mL dsDNA at λ_{ex} =529 nm and λ_{em}= 553 nm, at 4.5 slit width respectively. Fluorescence quench by DNA is indicated by the time of addition of dsDNA by a black arrow. Fluorescence trace is represented as the average of three replicates. Error bars represent standard error of the mean (*n*=3).

Following this positive result, a direct, whole-cell fluorometric efflux assay was conducted in triplicate against *E. coli* UTL2*mdfA::kan* cells loaded with 1 μM R6G. Cells harbouring pUC18/pAra/mdfA or pUC19/pBAD/mdfA_CL_V44C/V307C were investigated to determine whether MdfA and MdfA_CL_V44C/V307C could directly export R6G out of whole *E. coli* cells . Transport assays were assessed as described in section 2.9. As R6G fluorescence is quenched in the presence of DNA, direct efflux of R6G mediated by MdfA and MdfA_CL_V44C/V307C cells were characterised by an increase in R6G fluorescence over time as the substrate is expelled from the cells. Transport assays were performed across three biological replicates (Figure 10).

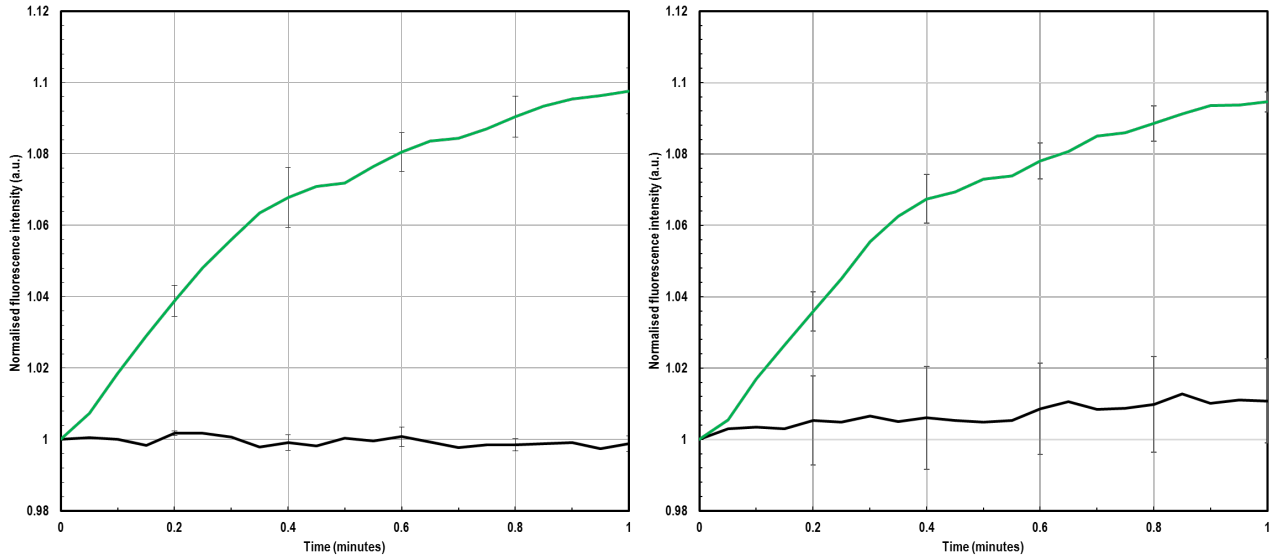

Figure 10. Rhodamine 6G transport mediated by MdfA (left) and MdfA_CL_V44C/V307C (right). Non-induced samples (black) and induced samples (green). Transport was initiated by 0.5M sodium formate at time point 0. The fluorescence traces represent the average of three independent experiments against 1 μM R6G at λ_{ex}= 529 nm and λ_{em} = 553 nm at slit widths of 4.5 nm. Error bars represent standard error of the mean (*n*=3).

The fluorescence transport assay demonstrated direct efflux of R6G mediated by MdfA. Moreover, the rate of transport mediated by the Cys-variant MdfA_CL_V44C/V307C was comparable to wild-type MdfA (Figure 10). To confirm that the change in fluorescence was related to transport and that the transport observed was energy dependent, experiments were performed where the protonophore CCCP was added after re-energisation. A representative trace demonstrating cell re-energisation with 0.5M sodium formate and inhibition of transport with CCCP to dissipate the electrochemical proton gradient is provided (Figure 11). This data confirms MdfA mediated overexpression is dependent on coupling to proton motive force, as previously determined by Edgar and Bibi in a whole-cell fluorometric efflux assay on MdfA against ethidium bromide (75). R6G appears to re-enter the cell after de-energisation of electrochemical gradient, whereby a further R6G quenching affect is

immediately observed after CCCP introduction. The rapid nature of the fluorescence reduction suggests that R6G fluorescence could be quenched when bound to the cell membrane.

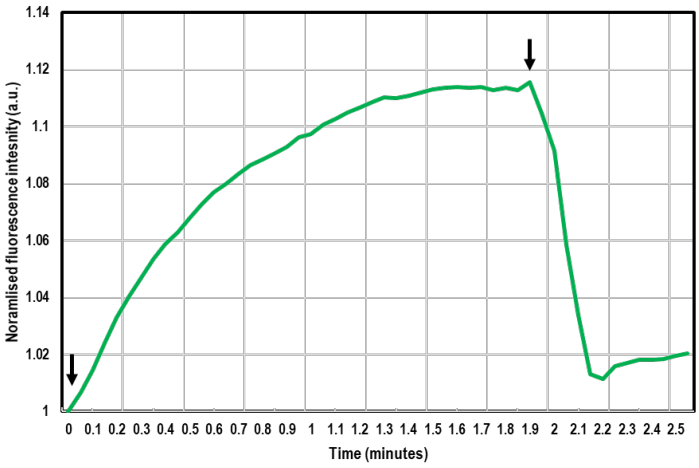

Figure 11. Representative trace of MdfA mediated R6G efflux. Arrows indicate addition of sodium formate to energise and CCCP to de-energise cells respectively, demonstrating proton-gradient dependent efflux of 1 μM R6G at λ_{ex}= 529 nm and λ_{em} =553 nm at slit widths 4.5 nm respectively.

Transport assays using bulk cell solutions demonstrated that R6G efflux is detectable. Furthermore, the application of these experiments has provided a direct visualisation of MdfA mediated transport of R6G in real-time. Moreover, no detectable difference between MdfA and Cys-variant MdfA_CL_V44C/V307C was observed. This indicates that MdfA_CL_V44C/V307C is active and may represent an ideal model of MdfA to characterise real-time alternating access of MdfA in single-molecule FRET assays while simultaneously visualizing R6G vectorial transport. The transport experiments were conducted in whole cells that include other efflux proteins. Therefore, to provide additional evidence for R6G being a direct substrate of MdfA, the next step for this project was to confirm that MdfA binds R6G using a tryptophan quenching assay. Furthermore, this experiment will yield important evidence to investigate whether the six amino acid modifications in the Cys-mutant MdfA_CL_V44C/V307C may have deleteriously impacted the binding affinity of the transporter for R6G.

3.3. Rhodamine 6G binding assay

3.3.1. Recombinant expression and purification of MdfA and MdfA_CL_V44C/V307C

To obtain pure MdfA and MdfA_CL_V44C/V307C to characterise their binding affinity to R6G, MdfA and MdfA_CL_V44C/V307C were overexpressed in an *E. coli* host harbouring a gene knockout for the native MdfA transporter (section 2.2). MdfA and MdfA_CL_V44C/V307C were overexpressed under saturating levels of inducer (0.2% v/v L-arabinose) to facilitate maximal expression under *araC*/P_{BAD} control (92). Purification was facilitated by immobilised metal affinity

chromatography, using Co^{2+} affinity to selectively chelate the hexa-His-tag at the C-terminus of MdfA and MdfA_CL_V44C/V307C with low affinity and high specificity, to allow for elution under mild imidazole salt conditions (93). Functional MdfA and MdfA_CL_V44C/V307C was successfully isolated after growing cells to 3L capacity, harvest and wash to remove excess media, before cell lysis using a French Press to disrupt *E. coli* cells. To extract membrane protein from the membrane, samples were treated with mild, non-ionic detergent 1.1% DDM, to avoid denaturation and achieve solubilisation of membrane proteins including MdfA (94). Solubilised membrane protein was loaded onto Co^{2+}-resin in buffer containing 5 mM imidazole at pH 8.0. The resin was washed using buffer containing 5 mM imidazole to remove non-specific proteins, and MdfA protein eluted using 150 mM imidazole. MdfA was purified at a final concentration of 0.2 mg per litre of culture. MdfA_CL_V44C/V307C was purified to a final yield of 0.6 mg per litre of culture. The three-fold difference in protein yield can be attributed to the observed better growth of *E. coli* cells harbouring pUC19/mdfA_CL_V44C/V307C. Isolated MdfA and MdfA_CL_V44C/V307C in SDS-PAGE gels was visualised with Coomassie Brilliant Blue SDS-PAGE (section 2.15) and verified by Western blot with a hexa-His-tag specific probe (Figure 12).

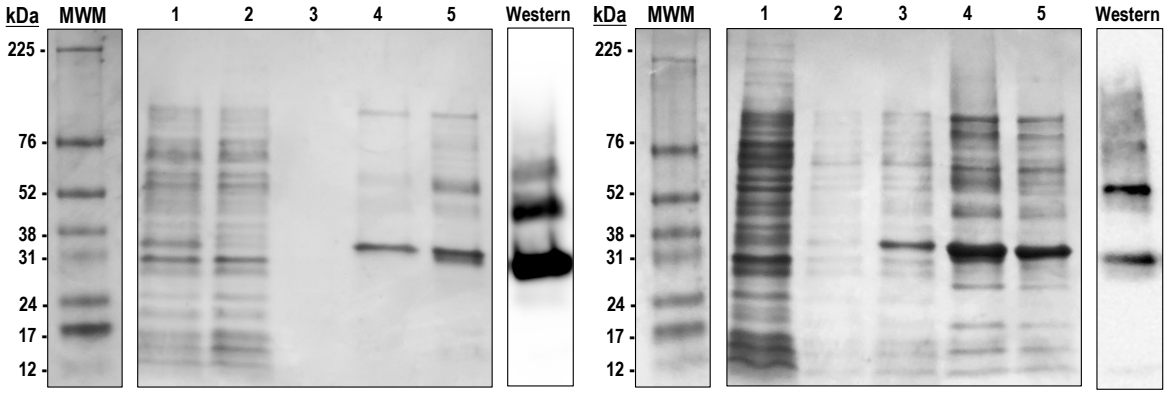

Figure 12. SDS-PAGE and western blot throughout protein purification. Left: MdfA; Right: MdfA_CL_V44C/V307C. SDS-PAGE: (1) DDM solubilised membrane fraction; (2) flow-through; (3) column wash; (4) void eluate; (5) eluate after 10-minute incubation with 150 mM imidazole. Gel was visualised with Coomassie Brilliant Blue R-250. Western: detection of recombinant protein at ~31 kDa was facilitated by use of a hexa-His-tag specific probe for direct detection of recombinant MdfA and MdfA_CL_V44C/V307C) engineered with a C-terminal hexa-His-tag (HisProbe-HRP™ , Thermo Scientific, USA).

Recombinant MdfA and MdfA_CL_V44C/V307C protein appears overexpressed at a lower apparent molecular weight of 31 kDa. The appearance of MdfA at a lower apparent molecular weight is typical for many membrane transport proteins and is likely due to binding of more SDS detergent during SDS-PAGE relative to their size than the soluble molecular weight markers, due to their higher hydrophobicity, thus giving them a greater net negative charge (95). This is supported by previous studies on MdfA that have also visualised wild-type MdfA to appear at a smaller molecular weight

of ~34 kDa rather than the predicted theoretical molecular weight of 44 kDa (77,96). Furthermore, the observation of higher-ordered bands corresponding to MdfA and MdfA_CL_V44C/V307C appear at ~60 kDa and ~90 kDa suggests presence of higher-ordered aggregates as verified by Western blotting (Figure 12).

3.3.2. Buffer Exchange Trials

The removal of imidazole prior to functional characterisation of MdfA is important as imidazole has been observed to bind to the binding site of multidrug binding proteins (97). Furthermore, due to the relatively low yield of protein, two methods buffer-exchange were investigated to determine a method that demonstrated the highest protein recovery method for recombinant MdfA and MdfA_CL_V44C/V307C.

Gel-filtration desalting columns offer a rapid method to separate small solutes from larger molecules was developed using size-exclusion chromatography (98). To facilitate separation, desalting columns are packed with a porous resin, allowing for solute size separation based on differential times to traverse the column (99). In these columns, larger molecules traverse columns at a fast rate, whereas small molecules elute at a slower rate as they traverse the pathways within porous resin beads that larger molecules are excluded from within the column (99). Two main methods of desalting have been commercialised, each with different benefits and disadvantages.

Spin-column desalting columns offer the most rapid desalting method without dilution as sample applied is subject to a small short-spin using centrifugal force to elute large molecules whilst trapping small molecules within the column. However, spin-columns risk trapping protein in the column, whilst also risking weak adsorption of protein onto the resin. Alternatively, desalting can be performed by gravity-flow, that depends on head-pressure of the buffer to push through applied sample down the desalting column. There is less risk of protein adsorption using this method, however, gravity-flow desalting is a considerably longer process and results in some dilution of the protein sample.

UV spectroscopy at A_{280} revealed 60% and 85% protein recovery for spin-column and gravity-flow methods respectively. Loss of significant protein under the spin-column desalting method is likely due to adsorption and entrapment of MdfA onto the desalting column. For gravity-flow, loss of 15% may be due to a weak affinity for the resin. SDS-PAGE and subsequent western blot verified the presence of MdfA after spin-column and gravity-flow (Figure 13).

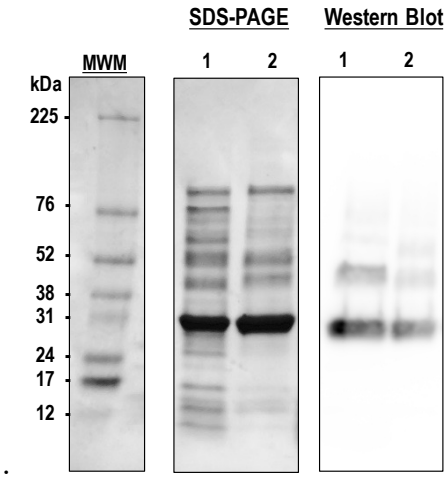

Figure 13. SDS-PAGE and western blot across two buffer-exchange methods against MdfA. Lanes (1) spin-column desalting method; (2) gravity-flow desalting method. All samples were quantified at A_{280} to account for protein loss after buffer exchange before spin-concentration to a final concentration of ~1 mg/mL for chemiluminescent detection of MdfA by western blot against hexa-His-tag probe (HisProbe-HRP™ , Thermo Scientific, USA).

3.2.3. Tryptophan quench assay

A tryptophan quenching assay was conducted to assess the binding affinity of MdfA for R6G. This experiment was deemed viable as MdfA contains ten native tryptophan (Trp) residues (Figure 14). Due to the highly anisotropic nature of tryptophan, intrinsic tryptophan fluorescence of a protein is highly sensitive to fluctuations in the local environment (81). As such, the capacity to selectively excite tryptophan amongst the fluorescent residues at λ= 295 nm and monitor changes in intrinsic tryptophan fluorescence emission λ= 340 nm provides a powerful tool to probe conformational changes in protein in response to substrate binding.

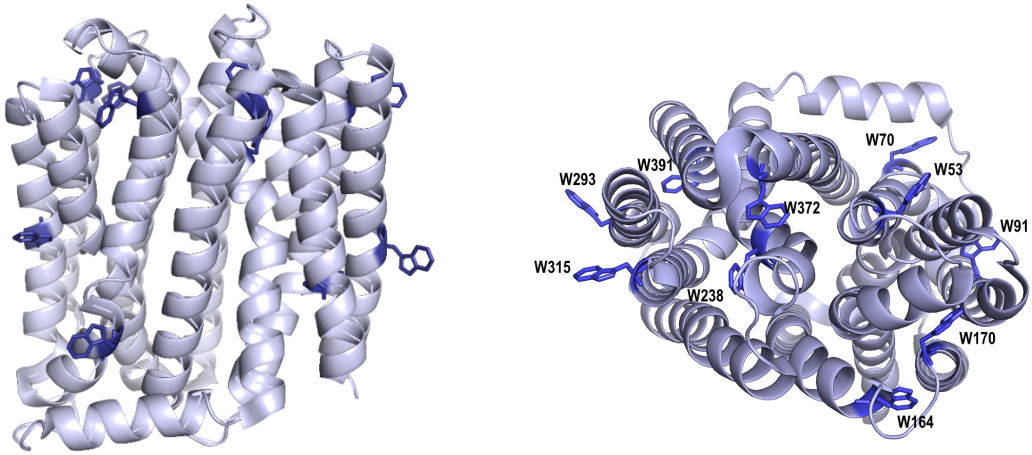

Figure 14. The locations of tryptophan residues present in MdfA [PDB:4ZOW] (56). MdfA Trp residues are highlighted in dark blue on the ribbon structure of MdfA. Figure built in PyMOL.

The tryptophan quenching assay against 1 μM of MdfA, revealed MdfA Trp fluorescence was readily quenched in the presence of low micromolar concentrations of R6G. This result was determined by

titration of R6G across low micromolar to high micromolar concentrations and minimal impact of fluorescence quench of R6G with free tryptophan at λ_{em} =340 nm (Figure 15).

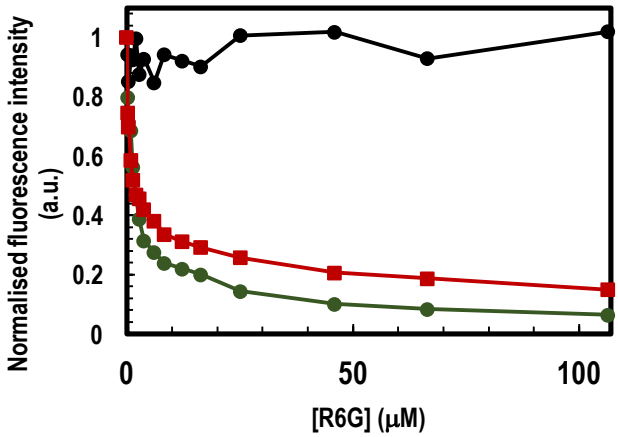

Figure 15. Tryptophan quench assay: MdfA (green), MdfA_CL_V44C/V307C (red) and free tryptophan (black) by titration of rhodamine 6G at λ_{ex}=295 nm and λ_{em} =340 nm.

To determine the binding affinity of R6G to MdfA, a dissociation constant (K_D) of 2.65± 0.69 μM was derived using curve fitting software KaleidaGraph (Synergy software) (section 2.16) (Figure 16), demonstrating that MdfA exhibits a tight binding affinity in the low micromolar range for R6G. The tryptophan quenching assay was also conducted on the Cys-variant mutant MdfA MdfA_CL_V44C/V307C, to determine if the six amino acid modifications on MdfA may have impacted on binding activity. Only a minor decrease in binding affinity was observed (K_D of 4.25 ±1.97μM) (Figure 16).

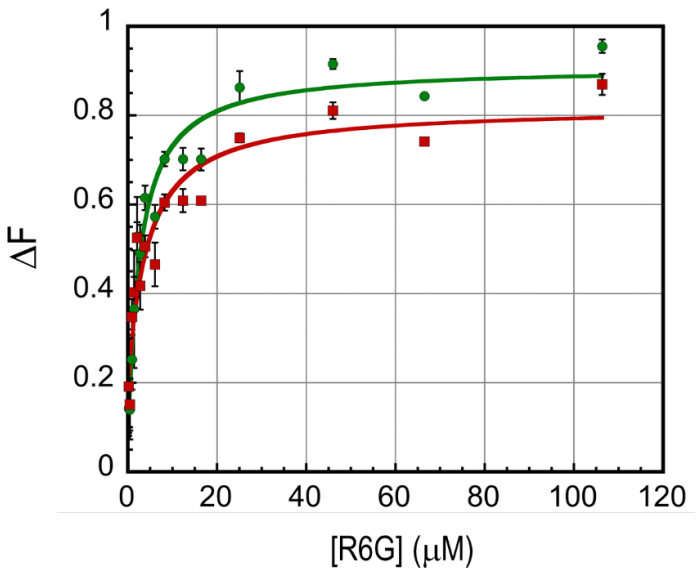

Figure 16. MdfA fluorescence corrected for inner filter effects (section 2.16) The proportion of quenchable fluorescence signal against corresponding free ligand concentration was fitted (section 2.16). The line of best fit derived from this data by KaleidaGraph determined a K_D value for R6G for MdfA (green) = 2.65 ±6.85 μM and MdfA_CL_V44C/V307C (red) = 4.25 μM ± 1.73 μM.

A low micromolar binding affinity for R6G may be expected for a multidrug efflux pump with broad-range substrate specificity, based on those seem for other multidrug efflux pumps with their substrates. A similar affinity for R6G was observed for two MATE efflux pumps that demonstrated broad-substrate specificity - NorM of *Neisseria gonorrhoeae* K_D= 3.4 ± 0.2 μM and YdhE of *E. coli*, K_D= 3.0 ± 0.2 μM (100).

3.4. Significance

The purpose of this chapter is to explore R6G as a substrate of MdfA. An initial screen for R6G resistance that could indicate this relationship was inconclusive. It was evident that more direct methods to determine R6G as a substrate for MdfA was needed. Fluorometric whole-cell assays demonstrate that MdfA overexpression led to directed R6G efflux out of *E. coli* cells. To probe if R6G as a substrate directly bound to MdfA and induced conformational change, purification of the membrane protein MdfA and a following a tryptophan quenching assay was conducted. MdfA was successfully purified in an active form to confirm that R6G bound as a substrate with low affinity. Following this positive result, an investigation was conducted to assess whether the Cys-variant MdfA_CL_V44C/V307C was a model candidate for single-molecule FRET investigations. Fluorometric transport assays, successful purification and the following tryptophan quenching assay reveal that Cys-variant was active and demonstrated similar transport and binding capacity as wild-type MdfA. The positive results from this section conclude that MdfA binds R6G, an extremely fluorescent and suitable dye for future single-molecule investigations of transport. Moreover, we conclude that MdfA_CL_V44C/V307C a Cys-variant of MdfA is an active mutant of MdfA that presents itself as a model candidate for sm-FRET study.

Chapter 4. Single-cell imaging of direct R6G efflux by MdfA_CL_V44C/V307C in *E. coli*

In Chapter 3, the Cys-variant MdfA was confirmed to directly transport and bind R6G in bulk fluorometry techniques. As a step-forward to observe R6G mediated efflux while simultaneously looking at conformational changes in the Cys-variant MdfA by single-molecule FRET, the direct observation of real-time R6G efflux mediated by Cys-variant MdfA at the single-cell level using single-molecule fluorescence microscopy was important. However, a single-cell fluorescence transport assay to directly observe fluorescence transport in live bacteria cells has not been developed. In this chapter, a novel single-cell transport assay, based on traditional whole-cell fluorometric transport assays, is developed for analysis of real-time fluorescence transport using wide-field single-molecule fluorescence microscopy.

4.1. Design of a microfluidic device for real-time imaging of R6G transport

To adapt the whole-cell fluorimetric transport assay for live cell imaging, a PDMS microfluidic flow cell was designed to enable flow to introduce and treat cell samples during live, time-lapse imaging of the transport assay. Firstly, to retain individual fluorescent *E. coli* cells within microfluidic flow channels for live imaging of transport, glass coverslips were treated with a strongly alkaline agent (5 M KOH). This treatment will allow for the activation of glass to promote a silanisation reaction with ATPES, an organofunctional alkoxysilane that provides a positive charge to facilitate strong bonding with bacterial LPS to promote adhesion and retention of bacterial cells within the microfluidic flow channels (101).

To generate a microfluidic flow cell, a PDMS elastomer was specifically chosen due to its biocompatibility, transparency, low auto-fluorescence and capability to permanently bond with APTES-derivatised glass coverslip (102,103). PDMS flow cells were custom-built at the Australian National Fabrication Facility (South Australian Node) to provide three flow channels to allow for three individual replicates to be performed per transport assay to be conducted. To facilitate entry of sample and manipulate introduction of sodium formate during live-cell imaging, sample inlet and outlet points were introduced simply by manually punching out small 3 mm wide sections of PDMS with a tissue cutter. The PDMS flow cell was activated by oxygen plasma treatment and immediately bonded to APTES coverslips to generate a sealed microfluidic device for sample introduction. The microfluidic device designed for single-cell transport assays is illustrated in Figure 17.

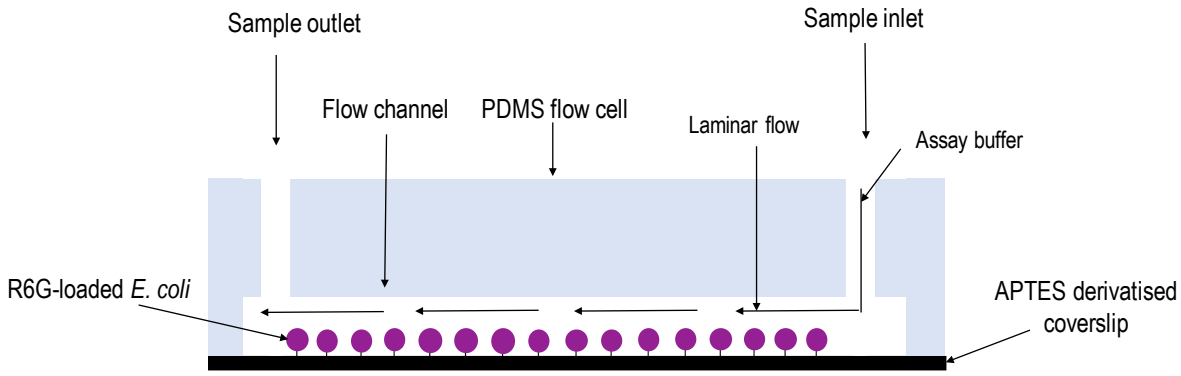

Figure 17. Schematic illustration of a designed microfluidic flow cell for a single-cell efflux assay. Illustration demonstrates the transparent nature of the PDMS flow cell to allow for direct imaging of intracellular R6G fluorescence within individual *E. coli* cells. Cross-section of one flow channel at ~30 mm x 0.1 mm x 0.5 mm (*l x h x w*) is represented. Manual sample inlets and outlets at ~20 µL volume capacity to facilitate sample introduction and aspiration to regulate sample flow. Individual *E. coli* cells are expected to adhere to APTES-derivatised coverslip, whilst introduction of assay buffer with exogenous energy at the sample inlet will induce laminar flow to distribute energy across individual single-cell *E. coli*. Direct observation of energy-dependent R6G transport can be visualised upon selective excitation of R6G and detection of R6G emission using time-lapse wide-field epifluorescence microscopy.

4.2. Culture preparation

Wide-field epifluorescence microscopy depends on the illumination of the whole-sample for time-lapse imaging of single cells. Therefore, it is important to reduce sources of background fluorescence. For this reason, *E. coli* DH5α cells were cultivated in EZ rich media, a transparent defined medium with low autofluorescence (104). To assess R6G mediated transport by Cys-variant overexpressing cells. *E. coli* DH5α cells overexpressing Cys-variant MdfA under 0.2% v/v L-arabinose was compared against a control that was repressed in the presence of 0.2% v/v D-glucose. R6G-loaded cells were prepared as described in section 2.10.

4.3. Time-lapse imaging of R6G transport by wide-field epifluorescence microscopy

Real-time imaging of live efflux of R6G was successfully conducted using a wide-field fluorescence microscope. To image and monitor changes in intracellular levels of R6G within individual *E. coli* cells, R6G loaded cells were introduced into the microfluidic device and incubated for one minute to promote cell adhesion to the APTES-modified glass slide. To image real-time changes in intracellular fluorescence of R6G, cells were imaged on a custom-built wide-field fluorescence microscope, whereby individual *E. coli* cells pre-loaded with R6G were excited at 514 nm at low power (20 W. cm^{-2}). To detect R6G emission, emission was collected between 525-555 nm, with no EM gain required.

Initial single-cell imaging experiments against R6G revealed a substantial population of *E. coli* cells to be weakly bound to the APTES coverslip. To remove excess non-adhered cells, a wash step was introduced to remove non-adherent cells by gently aspirating excess liquid within the flow channel and introduction of assay buffer. As the assay buffer is at neutral pH (20 mM HEPES, pH 7.0), this step was used as a control to observe whether *E. coli* cells demonstrated background transport of R6G. Time-lapse image acquisition of control washes against assay buffer were acquired for 1 minute every 100 ms. These experiments revealed no decrease in intracellular fluorescence intensity for both non-induced and induced *E. coli* cells (Figure 18). To initiate the transport assay, assay buffer was supplemented with 0.5M sodium formate and introduced into the flow cell at one end to introduce flow. Time-lapse imaging revealed R6G efflux for both non-induced and induced single-cell populations as a measure of decreased intracellular fluorescence intensity over-time as R6G is removed from the flow channel (Figure 18).

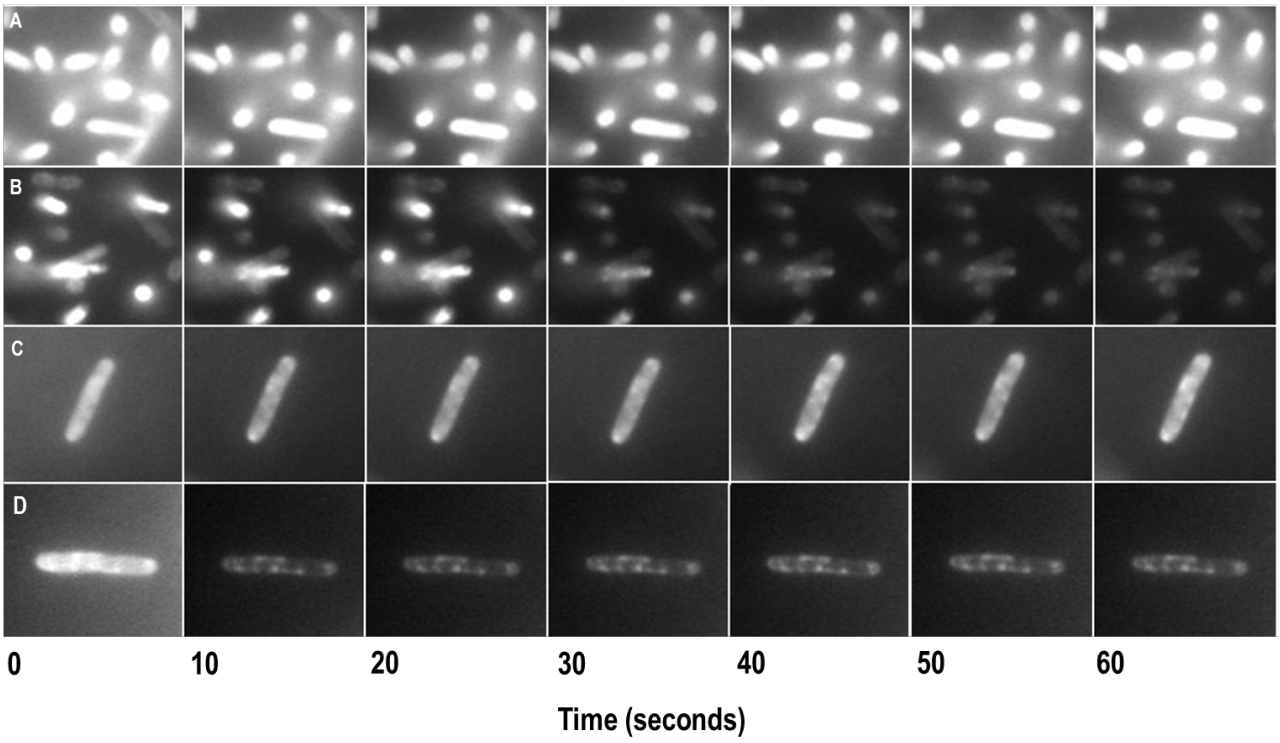

Figure 18. Time-lapse imaging of single-cell *E. coli* DH5α cells loaded with 1 μM R6G: (A) control in the absence of exogenous energy (B) control, treated with 0.5 M sodium formate; (C) MdfA_CL_V44C/V307C overexpressing cells in the absence of exogenous energy; (D) MdfA_CL_V44C/V307C overexpressing cells, treated with 0.5 M sodium formate. Time-lapse represented every 10 seconds. R6G excited at 514 nm, emission detected at 525-555 nm.

Image analysis revealed the presence of elongated cells in Cys-variant MdfA overexpressing cells but not in control cells. Elongation of bacterial cells is commonly seen under various types of stress (105–108), and is suggestive that overexpression of Cys-variant MdfA is deleterious for *E. coli*. The elongated cells significantly reduced cell number sampling size between the cell types. Sample size

for controls were *n*=25 and 38, respectively for control and sodium formate washes, whereas for larger cells adhered to the APTES did not provide room for multiple large cells, furthermore, length was determined to be arbitrarily elongated, reducing sample size to *n*=6 and *n*=8, respectively. The presence of elongated and dead *E. coli* cells further reduced cell sample size compared to control. Dead cells were identified as cells that did not export any R6G throughout the 60 seconds of imaging analysis. These cells were distinctly inactive in capacity to transport R6G out of the cell compared to controls. This data suggests toxic overexpression of MdfA_CL_V44C/V307C under the *araC*/P_{BAD} promotor and therefore expression of MdfA_CL_V44C/V307C under the *araC*/P_{BAD} control requires further optimisation. Image analysis also revealed the distinct presence of punctate fluorescent foci can be observed after 60 seconds of analysis in both control and induced samples. The precise mechanism that drives the formation of punctate foci with R6G in this context is unknown. However, R6G is a highly lipophilic and cationic dye and has been developed as a specific stain for phospholipids (109). Moreover, R6G has been characterised as a potent inhibitor of mitochondrial oxidative phosphorylation (110). Together, with the direct observation of membrane localised R6G foci close to the membrane may suggest a tight interaction of R6G with either lipids and/or biological machinery in the plasma membrane.

To determine the overall efflux of R6G, mean fluorescence intensity was analysed across all selected cells (excluding dead or vertical *E. coli* cells). Mean fluorescence intensity for each cell was analysed over 600 frames (60 seconds) to measure loss of intracellular fluorescence of R6G as a function of transport. To remove background fluctuations in fluorescence from the final data, mean fluorescence intensity of background was subtracted from all 600 frames. Fluorescence traces represent the normalised average over at least two replicates, where error bars represent the standard error of the mean where *n* = number of cells selected (Figure 19).

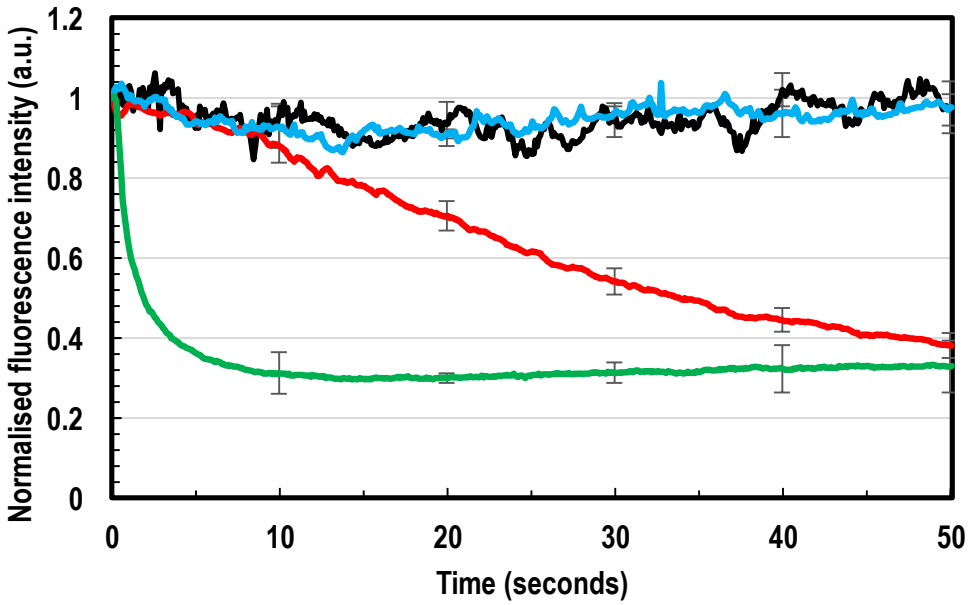

Figure 19. Mean intracellular fluorescence intensity vs time trajectory in single-cell transport assay against R6G. Control (non-induced) in the absence of exogeneous energy, *n*=25 (black); control in the presence of exogenous energy, *n*= 38 (red). MdfA_CL_V44C/V307C overexpressing cells (induced) in the absence of exogeneous energy, *n* = 6 (blue); MdfA_CL_V44C/V307C overexpressing cells (induced) in the presence of exogeneous energy, *n*= 8 (green). Error bars represent the standard error of the mean, where *n*= no. of cells selected.

Mean fluorescence trajectories demonstrate observable retention of intracellular R6G in de-energised control and induced cells. Overall R6G efflux was initiated in the presence of 0.5M sodium formate for both control and induced cells but with different initial rates of transport. Rapid efflux was observed for induced cells (<5 seconds), indicating Cys-variant MdfA overexpression demonstrated greatly improved transport of R6G compared to control. In the non-induced control cells, R6G efflux occurred over 50 seconds possibly due to basal expression levels of a repertoire of native MDR efflux pumps in *E. coli* DH5α and potentially some leaky expression of MdfA. Together, both the control and induced cells demonstrate total R6G efflux at ~30% R6G retention. This fluorescence retained can be expected if the foci observed between control and induced cells is due to irreversible or very tight R6G binding.

The single-cell efflux assay was successful in providing direct visual evidence that Cys-variant MdfA is active and can directly mediated R6G-efflux at the single-cell level. The positive result coming from this experiment confirms Cys-variant MdfA as a model candidate for real-time imaging of sm-FRET transport of R6G. Moreover, this experiment was particularly significant as the first study conducted to directly observe real-time transport of a fluorescence substrate by a multidrug efflux pump at the single-cell level. Therefore, the success of this experiment provides scope as a novel

transport assay to characterise multidrug efflux in individual bacterial cells using real-time wide-field epifluorescence microscopy.

4.4. Optimising the expression of a Cys-variant MdfA for single-cell transport analysis

The demonstrated success of the single-cell efflux assay provides significant scope for the characterisation of multidrug efflux transport at the single-cell level. The only problem incurred by the single-cell efflux assay was the severe impact on sample size number due to the presence of dead and elongated cells under induction with 0.2% v/v L-arabinose. The advantage of *araC*/P_{BAD} expression vector for membrane protein overexpression is the tight regulation of the gene construct, and furthermore, the tunability of protein overexpression ~1,200-fold (92). Toxic protein overexpression represents a major bottleneck in the functional characterisation of membrane proteins (111). Therefore, to improve on the developed single-cell efflux assay as a viable technique to characterise fluorescent substrate transport by multidrug efflux pumps, part of this thesis was dedicated to investigating various L-arabinose induction conditions to determine if cell viability, size and transport activity could be improved with lowered L-arabinose concentrations. These assays were conducted to optimise Cys-variant MdfA, MdfA_CL_V44C/V307C expression under *araC*/P_{BAD} control in *E. coli* UTL2*mdfA::kan* cells, due to the presence of a native MdfA knockout to reduce potential background efflux mediated by endogenously expressed chromosomal MdfA.

4.4.1. Investigation of inducer concentration on cell viability

To investigate cellular viability in *E. coli* DH5α cells expressing the Cys-variant MdfA after protein induction and the potential for *araC*/P_{BAD} tunability to improve cell viability for single-cell efflux assays, growth curves were conducted to monitor cellular growth at OD_{600}. Each growth curve was monitored for five hours after protein induction across ten-fold increasing inducer concentrations for comparison against a no-plasmid host control. Growth was observed to cease and the culture enter an immediate early stationary phase at the two highest inducer concentrations (0.2% and 0.02% v/v L-arabinose), whilst induction at an intermediate concentration (0.002% v/v L-arabinose) hampered normal cellular growth, but growth continued. The lowest concentration (0.0002% v/v L-arabinose) demonstrated negligible change to a parental host control (Figure 20).

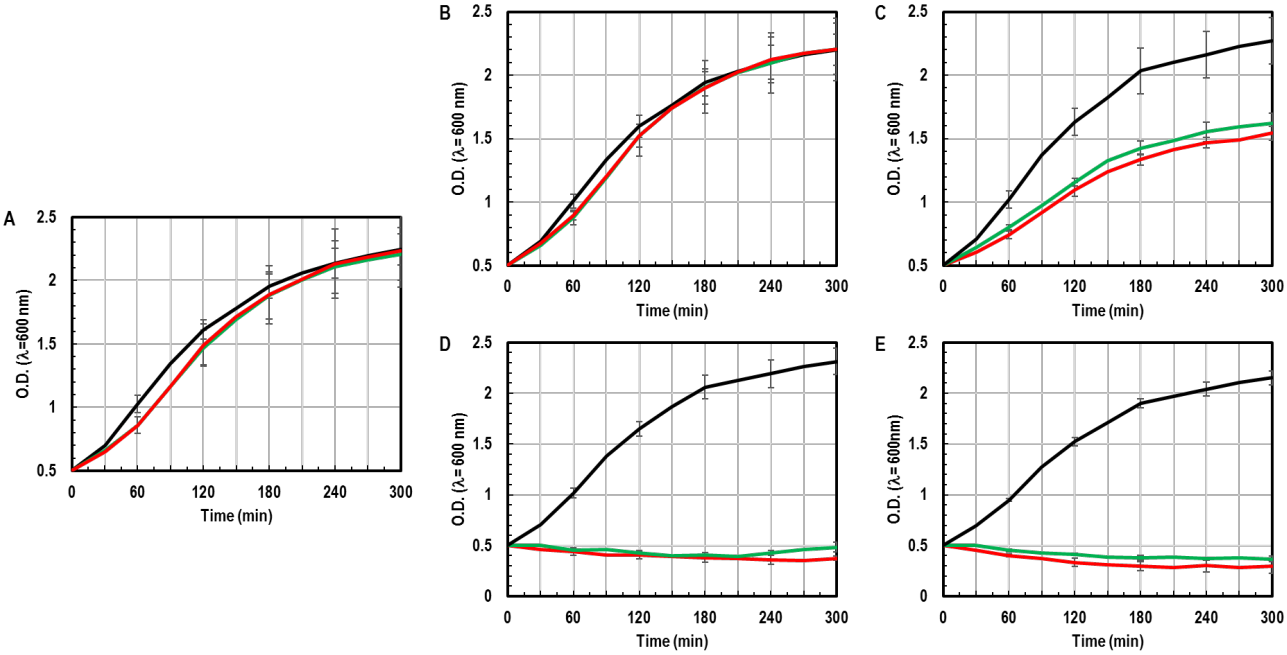

Figure 20. Influence of protein overexpression on cellular growth at OD_{600}. *E. coli* UTL2*mdfA::kan* host (black); MdfA (green); MdfA_CL_V44C/V307C (red). (A) pre-induction control; (B) induction with 0.0002% v/v L-arabinose; (C) induction with 0.002% v/v L-arabinose; (D) induction with 0.02% v/v L-arabinose; (E) induction with 0.2% v/v L-arabinose. Growth curves are representative of three independent growth curve experiments. Error bars represent standard error of the mean (*n*=3).

4.4.2. Scanning electron microscopy of induced cells

E. coli cell morphology during overexpression of Cys-variant MdfA was evaluated by scanning electron microscopy (SEM), to further investigate the unusually long *E. coli* cells formed after overexpressing this protein (section 2.12). Expression of MdfA_CL_V44C/V307C under the *araC*/P_{BAD} system was allowed to continue for one hour after L-arabinose induction. As expected, SEM revealed MdfA_CL_V44C/V307C-overexpressing cells are substantially elongated in the presence of highest inducer concentration (0.2% v/v L-arabinose) compared to lower inducer concentrations (0.0002% and 0.002% v/v L-arabinose) (Figure 21). L-arabinose at 0.02% v/v L-arabinose was not investigated due to similar cell viability profile to 0.2% v/v L-arabinose and limited sample capacity for gold-sputter coating (*n*=6) at the time of SEM analysis.

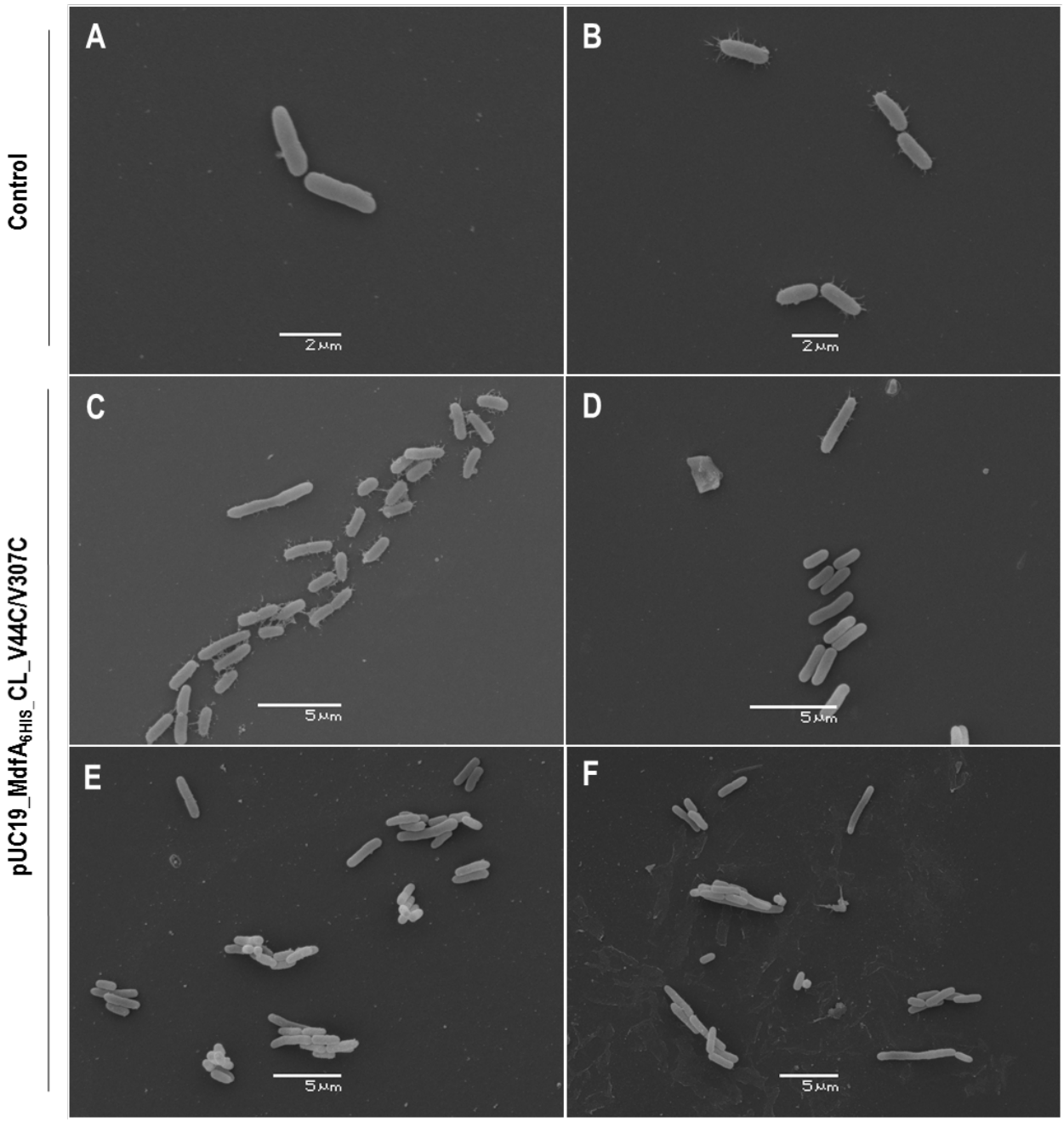

Figure 21. Scanning electron microscopy of *E. coli* UTL2*mdfA::kan* parental strain and strain overexpressing MdfA_CL_V44C/V307C at varying concentrations of L-arabinose inducer. (A) parental control, no inducer; (B) parental control, 0.2% v/v L-arabinose; (C) MdfA_CL_V44C/V307C, no inducer; (D) MdfA_CL_V44C/V307C overexpression at 0.0002% v/v L-arabinose; (E) MdfA_CL_V44C/V307C overexpression at 0.002% v/v L-arabinose; (F) MdfA_CL_V44C/V307C overexpression at 0.2% v/v L-arabinose.

E. coli UTL2*mdfA::kan* host and the MdfA_CL_V44C/V307C pre-induction control revealed an average mean length of 2.5 µm, normal for *E. coli* cells entering early stationary phase (2 µm) (Figure 22)(107). Average cell length of induced cells remained consistently across all conditions except for 0.2% v/v L-arabinose, which demonstrated a statistically significant 1.5-fold increase in average length to 3.8 µm compared to control cells at 2.5 µm ($p < 0.05$) (Figure 22).

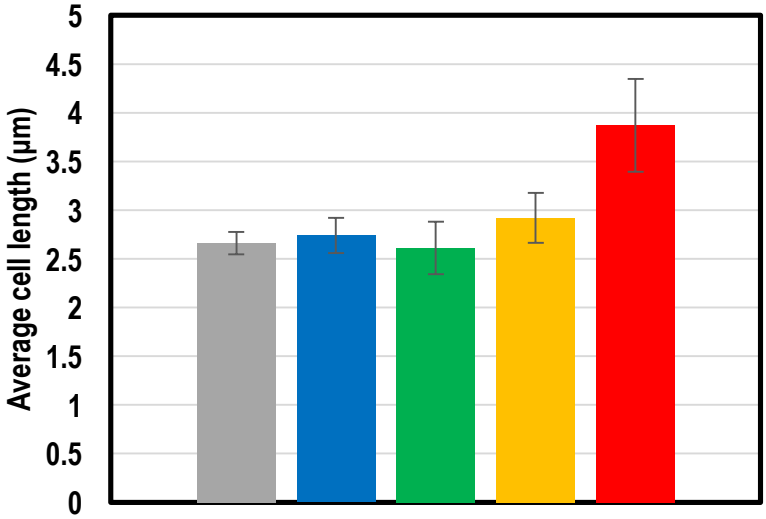

Figure 22. Measured *E. coli* cell lengths determined after 1-hour induction in L-arabinose. Parental control, *n*= 8 (grey); Cys-variant MdfA pre-induction control, *n*= 13 (blue); Induced Cys-variant MdfA – 0.0002% v/v L-arabinose, *n*= 13 (green); 0.002% v/v L-arabinose, *n*= 8 (yellow); 0.2% v/v L-arabinose, *n* = 17 (red). Error bars represent the standard error of the mean, whereby *n*= number of cells measured. Induction at 0.2% v/v L-arabinose indicate a statistically significant difference in average cell length in comparison to the parental control ($p < 0.05$), L-arabinose induction conditions <0.2%, yielded insignificant change in average cell length to parental control ($p > 0.05$)

SEM image analysis and measurement of a population of cells revealed that tuning arabinose-mediated induction to concentrations of <0.2% v/v L-arabinose was successful in reducing cellular length to an average of ~2.5 µm. It is clear from image analysis and average measurement of cellular length of *E. coli* at 0.2% v/v L-arabinose (Figure 21F, Figure 22) led to a population predominantly composed of elongated cells with an abnormally high average cellular length across cells that was statistically significant compared to the parental control ($p < 0.05$). MdfA_CL_V44C/V307C induction at lower L-arabinose conditions, 0.002% and 0.0002% did not reveal any significant deviation from the average cell length compared to the parental control ($p > 0.05$).

The SEM morphology data, combined with cell viability data from growth curve analysis (Figure 21F), reveal there is an unacceptable level of cellular elongation and a compromised cell viability at 0.2% v/v L-arabinose which has led to reduced sample size in the single-cell efflux assay. Therefore, 0.0002% or 0.002% v/v L-arabinose may provide a successful induction condition that improves cell viability and morphology to an appropriate level to improve sample size in a single-cell efflux assay.

4.4.3. Maximising the transport capacity of MdfA and MdfA_CL_V44C/V307C

To correlate whether inducer concentration also demonstrated an impact on transporter activity in whole-cells, the tunability of *araC*/P_{ARA} or *araC*/P_{BAD} promotor was assayed against whole-cell fluorescence transport assays against ethidium bromide, a well-characterised substrate of MdfA (112). The initial rate of ethidium bromide transport was assessed between wild-type MdfA and Cys-variant MdfA to account for a putative activity difference in EtBr transport and determine whether tunability of L-arabinose concentration could salvage transport activity across lowered L-arabinose overexpression conditions. Total transport of EtBr was hampered significantly at lowest (0.0002% v/v L-arabinose) and at highest inducer concentration (0.2% v/v L-arabinose), whereas transport assay showed a clear optimum at 0.002% v/v L-arabinose between wild-type and Cys-variant MdfA. Background transport in the pre-induction controls across both MdfA and MdfA_CL_V44C/V307C transport assays could represent endogenous, constitutively expressed MDR efflux pumps with specificity of ethidium bromide (88) (Figure 23).

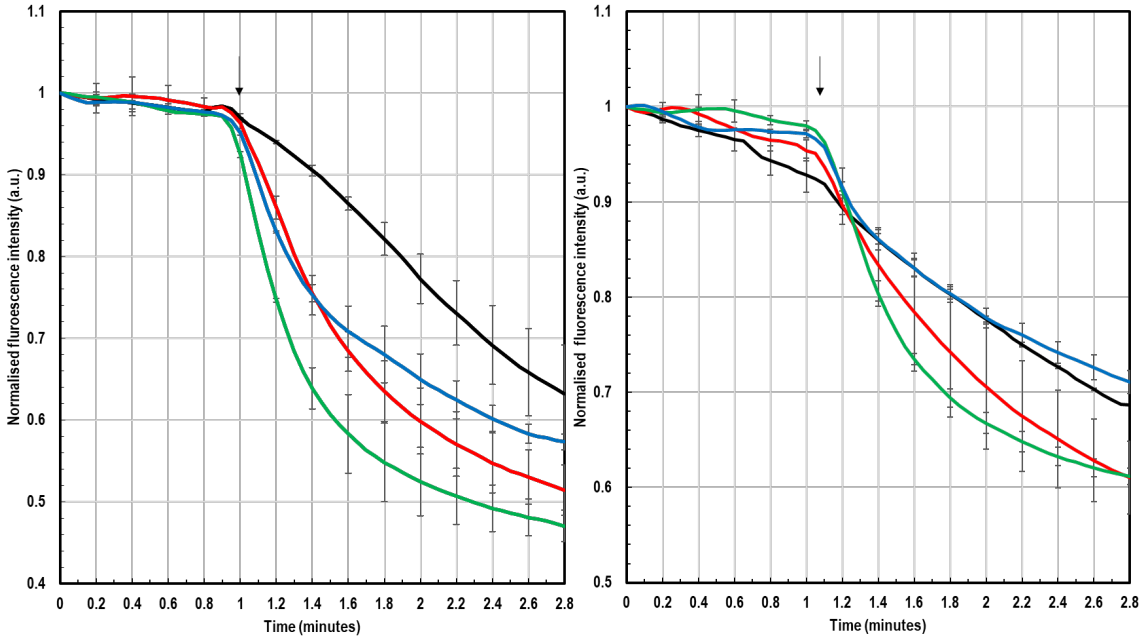

Figure 23. Ethidium bromide transport mediated by MdfA (left) and Cys-variant MdfA (right). Transport is shown for cultures induced with 0.2% (blue); 0.02% (red) 0.002% (green) and control (black). Transport is representative of three independent experiments; error bars represent standard error of the mean (*n*=3). Transport was initiated with the addition of sodium formate at ~1 minute, as indicated by a black arrow.

It is clear in this whole-cell fluorometric transport assay, that there is an optimum transport condition at 0.002% v/v L-arabinose across wild-type MdfA (53%) and MdfA_CL_V44C/V307C (38%). The differential transport between MdfA and MdfA_CL_V44C/V307C was also observed in the previous R6G transport assay (section 3.2). Together, both fluorimetric assays reveal that the difference in transport between MdfA and MdfA_CL_V44C/V307C is not considerable, it may indicate that there

is a reduction in the transport activity of the Cys-variant of MdfA. Transport activity between pre-induced and cells tested at 0.0002% v/v L-arabinose were negligible (data not shown). This is expected if there is insufficient quantity of MdfA and MdfA_CL_V44C/V307C being overexpressed at this condition. Highest inducer concentration tested at 0.2% v/v L-arabinose demonstrated a consistent 10% decrease in maximal transport rate across MdfA and MdfA_CL_V44C/V307C overexpressing cells. This possibly due to improperly folded protein as part of the cellular stress response (107). However, the lowered fluorescence change in the whole-cell transport assay can be attributed to the prevalence of elongated cells observed in the single-cell and SEM analysis that may impact on OD_{600} assessment of cell density. Furthermore, the presence of more DNA in each cell for which ethidium binds to may result in lowered fluorescence change detected using spectrofluorimetry.

4.5. Significance

The purpose of this chapter is to explore the development of a novel single-cell fluorescence transport assay based on a traditional whole-cell fluorometric transport assay workflow to allow for direct visualisation of R6G transport mediated by MdfA_CL_V44C/V307C in individual *E. coli* cells. The success of this novel assay confirmed that MdfA_CL_V44C/V307C is a model Cys-variant of MdfA to move forward for further investigation at the single-molecule level. This single-cell efflux assay provides scope as a new method to characterise multidrug efflux transport at the single-cell level using wide-field fluorescence microscopy. However, the only limitation observed in this assay was a reduced sample size number due to the toxic overexpression of MdfA_CL_V44C/V307C at 0.2% v/v L-arabinose. This condition demonstrated a significant impact on *E. coli* viability, physiology and transport activity against ethidium bromide in this section. The toxicity of the overexpression of MdfA and MdfA_CL_V44C/V307C was influenced by the concentration of L-arabinose, whereby tuning overall protein expression at an intermediate concentration of 0.002% v/v L-arabinose was deemed optimal for single-cell analysis of fluorescence transport by significant improvement in average cell length and cell viability which led to an observable improvement in ethidium bromide transport in a fluorometric transport assay. Ideally, it would be important to assess the level of protein expression across all sample types to identify total protein overexpressed across each condition to assess toxicity with level of total membrane protein expressed. Most importantly, this single-cell efflux assays should be repeated at 0.002% v/v L-arabinose to confirm the suitability of this induction condition to improve on sample size for single-cell analysis. Unfortunately, this was not able to be undertaken as part of this thesis, as at the time of this research, I was unable to access the specific equipment at our collaborators institution.

Chapter 5. Conclusions and future directions

5.1. Confirming Rhodamine 6G as a substrate for MdfA

MdfA is a H^+/multidrug antiporter of the MFS that has become a model for investigating secondary active transporters (113). In this study, MdfA was confirmed to transport R6G by the application of a fluorometric whole-cell transport assay, and was further confirmed to bind to R6G with low affinity in a tryptophan quench assay. Together, these two results to provide strong evidence for R6G as a substrate of MdfA. R6G is a highly fluorescent substrate well-suited for single-molecule fluorescence measurements (81). The extensive biochemical and structural evidence for the rocker-switch alternating access mechanism in MdfA coupled with the evidence for transport of R6G confirms the suitability of MdfA as a model multidrug efflux pump for investigations of secondary active transport using single-molecule FRET (56,78). The investigation of the single-molecule kinetics that drive the alternating access mechanism of MdfA during R6G transport will provide significant insight into the transient kinetics that drive the rocker-switch mechanism of MFS transporters (54). Furthermore, sm-FRET analysis of the alternating access mechanism of MdfA using R6G as a substrate for direct observation of transport may provide the first, direct evidence for a complete cycle of the alternating access mechanism of a secondary active transporter and the association of this cycle to the translocation of a fluorescent substrate.

5.2. Probing the activity of Cys-variant MdfA for sm-FRET

The first step towards single-molecule FRET is the site-specific labelling of a protein to accommodate the positioning of a donor and acceptor fluorophore. MdfA_CL_V44C/V307C is a Cys-less version of MdfA that harbours two independent cysteine residues at the apex of the N-terminal (V44C) and C-terminal (V307C) of MdfA. This mutant is ideal for the site-specific labelling by the conjugation reaction between a solvent accessible cysteine group and a maleimide-derivative dye at the apex of the two domains proposed to undergo the rocker-switch mechanism of alternating access (114). This mutant exhibits six amino acid modifications, therefore this study aimed to investigate the activity of the MdfA mutant to bind and transport R6G to assess for loss of activity against R6G. Whole-cell fluorometric transport assays against R6G demonstrated negligible difference between wild-type and mutant transport of R6G at 0.003%, whilst a tryptophan quenching assay revealed a 1.6-fold loss in binding affinity to R6G. Low-level loss of MdfA activity in this mutant compared to the wild-type was seen throughout this thesis. The Cys-less background of MdfA_CL_V44C/V307C harbours a C96A mutation, which has been recently proposed to participate in a well-conserved motif-B hydrogen-bond network across MFS transporters (56). As C96 is proposed to participate in a hydrogen-bond network of motif-B, it will be worthwhile investigating a C96S mutation to restore

the hydrogen-bond network of motif-B, whilst maintaining a Cys-less background for site-specific FRET labelling for sm-FRET studies.

5.3. Development of a single-cell fluorescence transport assay for multidrug efflux pumps

MdfA_CL_V44C/V307C is capable of direct binding and transport of R6G. As a step-forward to single-molecule FRET of the MdfA_CL_V44C/V307C mediated efflux of R6G, a single-cell transport assay was investigated to directly observe real-time R6G efflux in live *E. coli* cells using wide-field single-molecule fluorescence microscopy. The direct observation of rapid R6G efflux in *E. coli* provided strong evidence of R6G mediated transport by MdfA_CL_V44C/V307C against background efflux observed in the control. Therefore, there is scope for the use of MdfA_CL_V44C/V307C as a model of MdfA for single-molecule FRET.

Furthermore, the design of this experiment demonstrated the capacity to adapt a traditional whole-cell fluorometric assay for single-cell analysis, which reveals novel features of the physiology of a cell that may impact on assessment of fluorescence transport mediated by a multidrug efflux pump. In this case, dead cells could be selectively removed from a total population of cells for measurement of mean fluorescence transport. This feature cannot be facilitated in a whole-cell fluorometric transport assay that measures a whole population of cells within a sample. However, the sampling size of the single-cell assay was easily influenced by the elongation and presence of dead cells due to the toxic overexpression of MdfA_CL_V44C/V307C at 0.2% v/v L-arabinose. In further experiments stemming from the single-cell assay, we could correlate high inducer concentration with impaired cell viability and morphology to reduced efflux capacity in a whole-cell fluorometric transport assay against ethidium bromide. To improve on the single-cell efflux assay, a range of L-arabinose induction conditions were investigated to assess whether cell viability, cell length and transport activity could be improved at lowered L-arabinose inducer concentrations. In this study, tuning MdfA_CL_V44C/V307C overexpression to an intermediate concentration of 0.002% v/v L-arabinose was sufficient to promote a significantly improved transport activity in cells overexpressing the toxic membrane protein, whilst also demonstrating significant improvement to cell viability and average cell length suitable for single-cell analyses. Therefore, the success of the single-cell transport assay to directly observe MdfA_CL_V44C/V307C mediated R6G efflux and capacity to overcome the sampling size problem by tuning expression under an arabinose inducible promotor demonstrates that the single-cell fluorescence transport assay is a novel technique that may be suitable for the characterisation of multidrug efflux transport at the single-cell level.

5.4. Future Directions

The work described in this thesis provides multiple lines of evidence that MdfA can directly bind and transport R6G. Furthermore, this work also demonstrates that a Cys-variant MdfA_CL_V44C/V307C is active and represents a model Cys-variant of MdfA for sm-FRET analysis. Thus, the studies conducted in this thesis provide significant scope to move forward in the design of a sm-FRET experiment using MdfA_CL_V44C/V307C for single-molecule FRET analysis. The next step following these studies involves site specific FRET-pair labelling and ensemble FRET analysis to measure population FRET signals prior to single-molecule FRET analysis in parallel with R6G transport.

The Bibi laboratory group have data suggesting that amino acid positions 44 and 307 on MdfA to move relative to one another from the inward-facing conformation (27Å) to outward-facing conformation (40Å) (unpublished). To probe sensitive changes in distance of MdfA as the protein undergoes the alternating access mechanism, it is crucial to select a FRET pair that works close to the Förster working distance (R_0) of the cysteines in MdfA_CL_V44C/V307C (R_0 approximately at 3.35 nm). Ideally the donor and acceptor of a FRET pair also need to demonstrate similar quantum yield (>0.1), extinction coefficients and sufficient spectral separation to differentiate FRET signals from donor and acceptor within the FRET pair (66). To move forward with sm-FRET analysis, four prospective FRET pairs have been identified as suitable for labelling of the cysteine residues in MdfA_CL_V44C/V307C (Table 6).

Table 6. FRET pairs suitable for labelling MdfA at amino acid positions 44 and 307

Donor	Acceptor	Forster Radius (nm)	Reference
Alexa488	Cy3	3.8	(115)
Cy2	Cy5	3.8	(115)
ATTO425	ATTO725	3.5	ATTO-TEC (supplier)
ATTO490	ATTO725	3.7	ATTO-TEC (supplier)

Ensemble FRET analysis of detergent solubilised MdfA_CL_V44C/V307C labelled with a select FRET pair will be conducted to assess the labelling stoichiometry of a FRET pair donor/acceptor ratio and optimisation of experimental conditions that can be conducted at the ensemble level, e.g. examining FRET in the presence and absence of a saturating concentration of a substrate. Following initial results achieved in ensemble FRET against a non-fluorescent substrate, single-molecule FRET

of proteoliposome reconstituted MdfA_CL_V44C/V307C, pre-loaded with R6G can be assessed against a substrate using total internal fluorescence microscopy to directly observe vectorial transport of a fluorescent substrate in parallel to direct measurement of real-time domain movement as a function of FRET to provide the first visual evidence of the alternating access mechanism of a transport protein.

A part of this thesis was also dedicated to the design of a novel single-cell live efflux assay to directly observe R6G efflux mediated by MdfA_CL_V44C/V307C. The success of the single-cell efflux assay provided important evidence that MdfA_CL_V44C/V307C can transport R6G. There is ample scope to develop this technique by assessing well-characterised multidrug efflux members across clinically significant ABC, MFS, RND, MATE, SMR and PACE family members and using a range of fluorescent antimicrobials and toxic dyes. The single cell transport assay has the advantage of observing transport rates in single cells rather than a population average, and may be applied to examine substrates that are not differentially fluorescent inside and outside cells and are thus not well-suited for characterisation by whole-cell fluorometric transport assays.

5.5. Conclusion

Multidrug efflux pumps are a major class of multidrug resistance determinants in bacterial pathogens. Bacterial efflux pumps from six different transporter families are proposed to operate via alternating access transport mechanisms to export broad sets of clinically important antimicrobials. Transport under the alternating access mechanism is inherently dynamic. Single-molecule FRET offers an ideal platform to investigate real-time transient kinetics of this transport mechanism. However, the question of whether the alternating access mechanism of transport can be directly observed, and temporally-linked to substrate translocation has not been addressed in single-molecule FRET studies. To achieve this, the transporter of interest in a single-molecule FRET experiment must be able to export a fluorescent substrate that can be detected using single-molecule fluorescence microscopy. This thesis has contributed to this direction of study by confirming that MdfA, a model multidrug efflux pump of the MFS can directly bind and transport the highly fluorescent compound rhodamine 6G. Furthermore, this work has also confirmed the activity of MdfA_CL_V44C/V307C as a model Cys-variant of MdfA is viable for single-molecule FRET investigations. Additionally, a novel fluorescence transport assay has been developed and is being optimised, which provides scope for the characterisation of fluorescence transport of multidrug efflux pumps at the single-cell level for the first time.

References

1. Cooper GM. Transport of small molecules. In: The cell: A molecular approach. 2nd ed. Sunderland: Sinauer Associates; 2000.
2. Shi Y. Common folds and transport mechanisms of secondary active transporters. Annu Rev Biophys. 2013;42:51–72.
3. Ren Q, Paulsen IT. Comparative analyses of fundamental differences in membrane transport capabilities in prokaryotes and eukaryotes. PLoS Comput Biol. 2005;1(3):e27.
4. Saier MH. A functional-phylogenetic classification system for transmembrane solute transporters. Microbiol Mol Biol Rev. 2000;64(2):354–411.
5. Rees DC, Johnson E, Lewinson O. ABC transporters: the power to change. Nat Rev Mol Cell Biol. 2009;10(3):218–27.
6. Jardetzky O. Simple allosteric model for membrane pumps. Nature. 1966;211(5052):969–70.
7. Drew D, Boudker O. Shared molecular mechanisms of membrane transporters. Annu Rev Biochem. 2016;85:543–72.
8. World Health Organisation. Antimicrobial resistance: Global report on surveillance 2014. Geneva: World Health Organisation. 2014.
9. Blair JMA, Webber MA, Baylay AJ, Ogbolu DO, Piddock LJV. Molecular mechanisms of antibiotic resistance. Nat Rev Microbiol. 2015;13(1):42–51.
10. Nikaido H. Multidrug Resistance in Bacteria. Annu Rev Biochem. 2009;78(1):119–46.
11. Abraham EP, Chain E. An enzyme from bacteria able to destroy penicillin. Nature. 1940;146(3713):837–837.
12. Livermore DM. Defining an extended-spectrum β-lactamase. Clin Microbiol Infect. 2008;14(Suppl 1):3–10.
13. Queenan AM, Bush K. Carbapenemases: The versatile β-lactamases. Clin Microbiol Rev. 2007;20(3):440-58.
14. Blair JMA, Piddock LJV. How to measure export via bacterial multidrug resistance efflux pumps. MBio. 2016;7(4):e00840-16.
15. Davies J, Wright GD. Bacterial resistance to aminoglycoside antibiotics. Trends Microbiol. 1997;5(6):234–40.
16. Ubukata K, Nonoguchi R, Matsuhashi M, Konno M. Expression and inducibility in *Staphylococcus aureus* of the *mecA* gene, which encodes a methicillin-resistant *S. aureus*-specific penicillin-binding protein. J Bacteriol. 1989;171(5):2882–5.
17. Long KS, Poehlsgaard J, Kehrenberg C, Schwarz S, Vester B. The Cfr rRNA methyltransferase confers resistance to phenicols, lincosamides, oxazolidinones, pleuromutilins, and streptogramin A antibiotics. Antimicrob Agents Chemother. 2006;50(7):2500–5.
18. Eliopoulos GM, Huovinen P. Resistance to trimethoprim-sulfamethoxazole. Clin Infect Dis. 2001;32(11):1608–14.
19. Nikaido H. Prevention of drug access to bacterial targets: permeability barriers and active efflux. Science.1994;264(5157):382–8.
20. Delcour A. Outer membrane permeability and antibiotic resistance. Biochim Biophys Acta. 2009;1794(5):808–16.

21. Chevalier S, Bouffartigues E, Bodilis J, Maillot O, Lesouhaitier O, Feuilloley MGJ, et al. Structure, function and regulation of *Pseudomonas aeruginosa* porins. FEMS Microbiol Rev. 2017;41(5):598-722.

22. Hood MI, Jacobs AC, Sayood K, Dunman PM, Skaar EP. *Acinetobacter baumannii* increases tolerance to antibiotics in response to monovalent cations. Antimicrob Agents Chemother. 2010;54(3):1029–41.

23. Blanco P, Hernando-Amado S, Reales-Calderon J, Corona F, Lira F, Alcalde-Rico M, et al. Bacterial Multidrug Efflux Pumps: Much More Than Antibiotic Resistance Determinants. Microorganisms. 2016;4(1):14.

24. Higgins CF. Multiple molecular mechanisms for multidrug resistance transporters. Nature. 2007;446(7137):749–57.

25. Li X-Z, Mehrotra M. Role of Plasmid-Encoded Drug Efflux Pumps in Antimicrobial Resistance. In: Li X-Z, Elkins CA, Zgurskaya HI, editors. Efflux-Mediated Antimicrobial Resistance in Bacteria: Mechanisms, Regulation and Clincal Implications. Springer; 2016.

26. Saier MH, Paulsen IT. Phylogeny of multidrug transporters. Semin Cell Dev Biol [Internet]. 2001;12(3):205–13.

27. Hassan KA, Liu Q, Henderson PJF, Paulsen IT. Homologs of the *Acinetobacter baumannii* AceI transporter represent a new family of bacterial multidrug efflux systems. MBio. 2015;6(1):e01982-14.

28. Tseng TT, Gratwick KS, Kollman J, Park D, Nies DH, Goffeau A, et al. The RND permease superfamily: An ancient, ubiquitous and diverse family that includes human disease and development proteins. J Mol Microbiol Biotechnol. 1999;1(1):107–25.

29. Du D, Wang Z, James NR, Voss JE, Klimont E, Ohene-Agyei T, et al. Structure of the AcrAB–TolC multidrug efflux pump. Nature. 2014;509(7501):512–5.

30. Seeger MA, Schiefner A, Eicher T, Verrey F, Diederichs K, Pos KM. Structural asymmetry of AcrB trimer suggests a peristaltic pump mechanism. Science. 2006;313(5791):1295–8.

31. Murakami S, Nakashima R, Yamashita E, Matsumoto T, Yamaguchi A. Crystal structures of a multidrug transporter reveal a functionally rotating mechanism. Nature. 2006;443(7108):173–9.

32. Eicher T, Seeger MA, Anselmi C, Zhou W, Brandstätter L, Verrey F, et al. Coupling of remote alternating-access transport mechanisms for protons and substrates in the multidrug efflux pump AcrB. Elife. 2014;3:e03145.

33. Wang Z, Fan G, Hryc CF, Blaza JN, Serysheva II, Schmid MF, et al. An allosteric transport mechanism for the AcrAB-TolC multidrug efflux pump. Elife. 2017;6:e24905.

34. Dawson RJP, Locher KP. Structure of a bacterial multidrug ABC transporter. Nature. 2006;443(7108):180–5.

35. Ward A, Reyes CL, Yu J, Roth CB, Chang G. Flexibility in the ABC transporter MsbA: Alternating access with a twist. Proc Natl Acad Sci U S A. 2007;104(48):19005–10.

36. Choudhury HG, Tong Z, Mathavan I, Li Y, Iwata S, Zirah S, et al. Structure of an antibacterial peptide ATP-binding cassette transporter in a novel outward occluded state. Proc Natl Acad Sci U S A. 2014;111(25):9145–50.

37. van Veen HW. Bacterial ABC multidrug exporters: From shared proteins motifs and features to diversity in molecular mechanisms. In: George AM, editor. ABC transporters—40 years on. Cham: Springer; 2016.

38. Dawson RJP, Locher KP. Structure of the multidrug ABC transporter Sav1866 from *Staphylococcus aureus* in complex with AMP-PNP. FEBS Lett. 2007;581(5):935–8.

39. Omote H, Hiasa M, Matsumoto T, Otsuka M, Moriyama Y. The MATE proteins as fundamental transporters of metabolic and xenobiotic organic cations. Trends Pharmacol Sci. 2006;27(11):587–93.

40. Lu M, Radchenko M, Symersky J, Nie R, Guo Y. Structural insights into H+-coupled multidrug extrusion by a MATE transporter. Nat Struct Mol Biol. 2013;20(11):1310–7.

41. Lu M, Symersky J, Radchenko M, Koide A, Guo Y, Nie R, et al. Structures of a Na+-coupled, substrate-bound MATE multidrug transporter. Proc Natl Acad Sci. 2013;110(6):2099–104.

42. Jin Y, Nair A, Van Veen HW. Multidrug transport protein NorM from *Vibrio cholerae* simultaneously couples to sodium- and proton-motive force. J Biol Chem. 2014;289(21):14624–32.

43. He X, Szewczyk P, Karyakin A, Evin M, Hong W-X, Zhang Q, et al. Structure of a cation-bound multidrug and toxic compound extrusion transporter. Nature. 2010;467(7318):991–4.

44. Tanaka Y, Hipolito CJ, Maturana AD, Ito K, Kuroda T, Higuchi T, et al. Structural basis for the drug extrusion mechanism by a MATE multidrug transporter. Nature. 2013;496(7444):247–51.

45. Littlejohn TG, Paulsen IT, Gillespie MT, Tennent JM, Midgley M, Jones IG, et al. Substrate specificity and energetics of antiseptic and disinfectant resistance in *Staphylococcus aureus*. FEMS Microbiol Lett. 1992;95(2–3):259–65.

46. Paulsen IT, Brown MH, Skurray RA. Proton-dependent multidrug efflux systems. Microbiol Rev. 1996;60(4):575–608.

47. Ubarretxena-Belandia I, Baldwin JM, Schuldiner S, Tate CG. Three-dimensional structure of the bacterial multidrug transporter EmrE shows it is an asymmetric homodimer. EMBO J. 2003;22(23):6175–81.

48. Chen Y-J, Pornillos O, Lieu S, Ma C, Chen AP, Chang G. X-ray structure of EmrE supports dual topology model. Proc Natl Acad Sci U S A [Internet]. 2007;104(48):18999–9004.

49. Morrison EA, DeKoster GT, Dutta S, Vafabakhsh R, Clarkson MW, Bahl A, et al. Antiparallel EmrE exports drugs by exchanging between asymmetric structures. Nature. 2011;481(7379):45–50.

50. Dastvan R, Fischer AW, Mishra S, Meiler J, Mchaourab HS. Protonation-dependent conformational dynamics of the multidrug transporter EmrE. Proc Natl Acad Sci U S A. 2016;113(5):1220–5.

51. Fleishman SJ, Harrington SE, Enosh A, Halperin D, Tate CG, Ben-Tal N. Quasi-symmetry in the cryo-em structure of EmrE provides the key to modeling its transmembrane domain. J Mol Biol. 2006;364(1):54–67.

52. Saier MH, Beatty JT, Goffeau A, Harley KT, Heijne WH, Huang S-CC, et al. The major facilitator superfamily. J Mol Microbiol Biotechnol. 1999;1(2):257–79.

53. Pao SS, Paulsen IT, Saier MH. Major facilitator superfamily. Microbiol Mol Biol Rev. 1998;62(1):1–34.

54. Law CJ, Maloney PC, Wang DN. Ins and outs of major facilitator superfamily antiporters. Annu Rev Microbiol. 2008;62(1):289–305.

55. Yin Y. Structure of the multidrug transporter EmrD from *Escherichia coli*. Science. 2006;312(5774):741–4.

56. Heng J, Zhao Y, Liu M, Liu Y, Fan J, Wang X, et al. Substrate-bound structure of the *E. coli* multidrug resistance transporter MdfA. Cell Res. 2015;25(9):1060–73.

57. Jiang D, Zhao Y, Wang X, Fan J, Heng J, Liu X, et al. Structure of the YajR transporter suggests a transport mechanism based on the conservered motif A. Proc Natl Acad Sci U S A. 2013;110:14664–9.

58. Hassan KA, Jackson SM, Penesyan A, Patching SG, Tetu SG, Eijkelkamp BA, et al. Transcriptomic and biochemical analyses identify a family of chlorhexidine efflux proteins. Proc Natl Acad Sci U S A. 2013;110(50):20254–9.

59. Murakami S. Structure and transport mechanisms of RND efflux pumps. In: Li X-Z, Elkins CA, Zgurskaya HI, editors. Efflux-mediated antimicrobial resistance in bacteria: Mechanisms, regulation and clincal implications. Springer; 2016.

60. Nair AV, Lee KW, van Veen HW. Structural and functional landscape of MFS and MATE efflux pumps. In: Li X-Z, Elkins CA, Zgurskaya HI, editors. Efflux-mediated antimicrobial resistance in bacteria: Mechanisms, regulation and clincal implications. Springer; 2016.

61. Bay DC, Turner RJ. Small multidrug resistance efflux pumps. In: Li X-Z, Elkins CA, Zgurskaya HI, editors. Efflux-mediated antimicrobial resistance in bacteria: Mechanisms, regulation and clincal implications. Springer; 2016.

62. Orelle C, Jault JM. Structures and transport mechanisms of the ABC efflux pumps. In: Li X-Z, Elkins CA, Zgurskaya HI, editors. Efflux-mediated antimicrobial resistance in bacteria: Mechanisms, regulation and clincal implications. Springer; 2016.

63. Wong K, Ma J, Rothnie A, Biggin PC, Kerr ID. Towards understanding promiscuity in multidrug efflux pumps. Trends Biochem Sci. 2014;39(1):8–16.

64. Stansfeld PJ, Sansom MSP. Molecular simulation approaches to membrane proteins. Structure. 2011;19(11):1562–72.

65. Oijen AM Van, Dixon NE. Probing molecular choreography through single-molecule biochemistry. Nat Struct Mol Biol. 2015;22(12):948–52.

66. Roy R, Hohng S, Ha T. A practical guide to single-molecule FRET. Nat Methods. 2008;5(6):507–16.

67. Wu PG, Brand L. Resonance energy transfer: Methods and applications. Anal Biochem.. 1994;218(1):1-13.

68. Stryer L. Fluorescence energy transfer as a spectroscopic ruler. Annu Rev Biochem. 1978;47(5):819-46.

69. Stryer L, Haugland RP. Energy transfer: a spectroscopic ruler. Proc Natl Acad Sci U S A. 1967;58(2):719–26.

70. Ha T. Single-molecule fluorescence resonance energy transfer. Methods. 2001;25(1):78-86.

71. Erkens GB, Hänelt I, Goudsmits JMH, Slotboom DJ, van Oijen AM. Unsynchronised subunit motion in single trimeric sodium-coupled aspartate transporters. Nature. 2013;502:119–23.

72. Akyuz N, Altman RB, Blanchard SC, Boudker O. Transport dynamics in a glutamate transproter homologue. Nature. 2013;502(7469):114–8.

73. Zhao Y, Terry DS, Shi L, Quick M, Weinstein H, Blanchard SC, et al. Substrate-modulated gating dynamics in Na+-coupled neurotransmitter transporter homologue. Nature. 2011;474(7349):109–13.

74. Verhalen B, Ernst S, Börsch M, Wilkens S. Dynamic ligand-induced conformational rearrangements in P-glycoprotein as probed by fluorescence resonance energy transfer spectroscopy. J Biol Chem. 2012;287(2):1112–27.

75. Edgar R, Bibi E. MdfA, an *Escherichia coli* multidrug resistance protein with an extraordinarily broad spectrum of drug recognition. J Bacteriol. 1997;179(7):2274–80.

76. Adler J, Bibi E. Membrane topology of the multidrug transporter MdfA: Complementary gene fusion studies reveal a nonessential C-terminal domain. J Bacteriol. 2002;184(12):3313–20.

77. Sigal N, Fluman N, Siemion S, Bibi E. The secondary multidrug/proton antiporter MdfA tolerates displacements of an essential negatively charged side chain. J Biol Chem. 2009;284(11):6966–71.

78. Fluman N, Ryan CM, Whitelegge JP, Bibi E. Dissection of mechanistic principles of a secondary multidrug efflux protein. Mol Cell. 2012;47(5):777–87.

79. Adler J, Bibi E. Determinants of substrate recognition by the *Escherichia coli* multidrug transporter MdfA identified on both sides of the membrane. J Biol Chem. 2004;279(10):8957–65.

80. Kubin RF, Fletcher AN. Fluorescence quantum yields of some rhodamine dyes. J Lumin. 1982;27(4):455–62.

81. Lakowicz JR. Principles of fluorescence spectroscopy. 3rd ed. Springer. New York; 2006.

82. Edgar R, Bibi E. A single membrane-embedded negative charge is critical for recognizing positively charged drugs by the *Escherichia coli* multidrug resistance protein MdfA. EMBO J. 1999;18(4):822–32.

83. Wiegand I, Hilpert K, Hancock REW. Agar and broth dilution methods to determine the minimal inhibitory concentration (MIC) of antimicrobial substances. Nat Protoc. 2008;3(2):163–75.

84. Robinson A, Mcdonald JP, Caldas VEA, Patel M, Wood A, Punter CM, et al. Regulation of Mutagenic DNA Polymerase V Activation in Space and Time. PLoS Genet. 2015;11(8):e1005482.

85. Schneider CA, Rasband WS, Eliceiri KW. NIH Image to ImageJ: 25 years of image analysis. Nat Methods. 2012;9(7):671–5.

86. Fluman N, Adler J, Rotenberg SA, Brown MH, Bibi E. Export of a single drug molecule in two transport cycles by a multidrug efflux pump. Nat Commun. 2014;5(May):4615.

87. Gasteiger E, Hoogland C, Gattiker A, Duvaud S, Wilkins M., Appel R., et al. Protein identification and analysis tools on the ExPASy Server. In: Walker J., editor. The proteomics protocols handbook. Totowa: Humana Press; 2005. p. 571–607.

88. Tal N, Schuldiner S. A coordinated network of transporters with overlapping specificities provides a robust survival strategy. Proc Natl Acad Sci U S A. 2009;106(22):9051–6.

89. Nishino K, Yamaguchi A. Analysis of a complete library of putative drug transporter genes in *Escherichia coli*. J Bacteriol. 2001;183(20):5803–12.

90. Letuta SN, Ketsle GA., Levshin LV., Nikiyan AN, Davydova OK. A study of the interaction of rhodamine 6G with DNA by spectrophotometry and probe microscopy. Opt Spectrosc. 2002;93(6):844–7.

91. Al Masum A, Chakraborty M, Ghosh S, Laha D, Karmakar P, Islam MM, et al. Biochemical activity of a fluorescent dye rhodamine 6G: Molecular modeling, electrochemical, spectroscopic and thermodynamic studies. J Photochem Photobiol B. 2016;164:369–79.

92. Guzman L, Belin D, Carson MJ. Tight Regulation, Modulation, and High-Level Expression by Vectors Containing the Arabinose PBAD Promoter. J Bacteriol. 1995;177(14):4121–30.

93. Bornhorst JA, Falke JJ. Purification of Proteins Using Polyhistidine Affinity Tags. Methods Enzymol. 2000;326:245–54.

94. Prive GG. Detergents for the stabilization and crystallization of membrane proteins. Methods. 2007;41(4):388–97.

95. Rath A, Glibowicka M, Nadeau VG, Chen G, Deber CM. Detergent binding explains anomalous SDS-PAGE migration of membrane proteins. Proc Natl Acad Sci U S A. 2009;106(6):1760–5.

96. Tirosh O, Sigal N, Gelman A, Sahar N, Fluman N, Siemion S, et al. Manipulating the drug/proton antiport stoichiometry of the secondary multidrug transporter MdfA. Proc Natl Acad Sci U S A. 2012;109(31):12473–8.

97. Peters KM, Brooks BE, Schumacher MA, Skurray RA, Brennan RG, Brown MH. A single acidic residue can guide binding site selection but does not govern QacR cationic-drug affinity. PLoS One. 2011;6(1): e15974.

98. Porath J, Flodin P. Gel filtration: A method for desalting and group seperation. Nature. 1959;183(4653):1657–9.

99. Sheehan D. Physical biochemistry: principles and applications. 2nd ed. Wiley-Blackwell; 2009.

100. Long F, Rouquette-Loughlin C, Shafer WM, Yu EW. Functional cloning and characterization of the multidrug efflux pumps NorM from *Neisseria gonorrhoeae* and YdhE from *Escherichia coli*. Antimicrob Agents Chemother. 2008;52(9):3052–60.

101. Lu Q, Wang J, Faghihnejad A, Zeng H, Liu Y. Understanding the molecular interactions of lipopolysaccharides during *E. coli* initial adhesion with a surface forces apparatus. Soft Matter. 2011;7(19):9366-9379.

102. Velve-Casquillas G, Le Berre M, Piel M, Tran PT. Microfluidic tools for cell biological research. Nano Today. 2010;5(1):28–47.

103. Aran K, Sasso LA, Kamdar N, Zahn JD. Irreversible, direct bonding of nanoporous polymer membranes to PDMS or glass microdevices. Lab Chip. 2010;10(5):548-52.

104. Neidhardt FC, Bloch PL, Smith DF. Culture medium for enterobacteria. J Bacteriol. 1974;119(3):736–47.

105. Cushnie TPT, O'Driscoll NH, Lamb AJ. Morphological and ultrastructural changes in bacterial cells as an indicator of antibacterial mechanism of action. Cell Mol Life Sci. 2016;73(23):4471–92.

106. Justice SS, Hunstad DA, Cegelski L, Hultgren SJ. Morphological plasticity as a bacterial survival strategy. Nat Rev Microbiol. 2008;6:162–8.

107. Gubellini F, Verdon G, Karpowich NK, Luff JD, Boël G, Gauthier N, et al. Physiological response to membrane protein overexpression in *E. coli*. Mol Cell Proteomics. 2011;10(10):M111.007930.

108. Wainwright M, Canham LT, Reeves CL. Morphological changes (including filamentation) in *Escherichia coli* grown under starvation conditions on silicon wafers and other surfaces. Lett Appl Microbiol. 1999;29(4):224–7.

109. Dittmer JC, Lester RL. A simple, specific spray for the detection of phospholipids on thin-layer chromatograms. J Lipid Res. 1964;(5):126–7.

110. Gear AR. Rhodamine 6G. A potent inhibitor of mitochondrial oxidative phosphorylation. J Biol Chem. 1974;249(11):3628–37.

111. Wagner S, Baars L, Ytterberg AJ, Klussmeier A, Wagner CS, Nord O, et al. Consequences of membrane protein overexpression in *Escherichia coli*. Mol Cell Proteomics. 2007;6(9):1527–50.

112. Lewinson O, Adler J, Poelarends GJ, Mazurkiewicz P, Driessen AJM, Bibi E. The *Escherichia coli* multidrug transporter MdfA catalyzes both electrogenic and electroneutral transport reactions. Proc Natl Acad Sci U S A. 2003;100(4):1667–72.

113. Sigal N, Cohen-Karni D, Siemion S, Bibi E. MdfA from *Escherichia coli*, a model protein for studying secondary multidrug transport. J Mol Microbiol Biotechnol. 2006;11(6):308-17.

114. Kim Y, Ho SO, Gassman NR, Korlann Y, Landorf E V., Collart FR, et al. Efficient site-specific labeling of proteins via cysteines. Bioconjug Chem. 2008;19(3):786–91.

115. Hartmann RK, Bindereif A, Schön A, Westhof E. Studying RNA using single molecule fluorescence resonance energy transfer. In: Handbook of RNA Biochemistry. Wiley; 2015.